"Aptamer-peptide conjugates as a new strategy to modulate human α-thrombin binding affinity". Anna Aviñó, Andreia F. Jorge, César S. Huertas, Tânia F. G. G. Cova, Alberto Pais, Laura M. Lechuga, Ramon Eritja and Carme Fabrega. BBA- General Subjects, 1863(10), 1619-1630 (2019). Doi: 10.1016/j.bbagen.2019.06.014.

Aptamer-peptide conjugates as a new strategy to modulate human α-thrombin binding affinity

Anna Aviñó[a,d], *Andreia F. Jorge*[b], *César S. Huertas*[c1], *Tânia F. G. G. Cova*[b], *Alberto Pais*[b], *Laura M. Lechuga*[c,d], *Ramon Eritja*[a,d,*] *and Carme Fabrega*[a,d,*]

[a]Institute for Advanced Chemistry of Catalonia (IQAC-CSIC), Jordi Girona 18-26, E-08034 Barcelona, Spain.

[b]CQC, Department of Chemistry, University of Coimbra, Rua Larga, 3004-535 Coimbra, Portugal.

[c]Catalan Institute of Nanoscience and Nanotechnology (ICN2), CSIC, ICN2 Building, Campus UAB, Bellaterra, 08193 Barcelona, Spain.

[d]Networking Center on Bioengineering, Biomaterials and Nanomedicine (CIBER-BBN), Jordi Girona 18-26, E-08034 Barcelona, Spain.

Corresponding Author at: Institute for Advanced Chemistry of Catalonia (IQAC-CSIC), Jordi Girona 18-26, E-08034 Barcelona, Spain.

Email; recgma@cid.csic.es (R. Eritja), cgcnqb@cid.csic.es (C. Fàbrega).

Present address.

[1]School of Engineering, RMIT University, Melbourne, VIC 3001 (Australia) (C. S.H.).

ABSTRACT

Aptamers are single-stranded RNA or DNA molecules that specifically recognize their targets and have proven valuable for functionalizing sensitive biosensors. α-thrombin is a trypsin-like serine proteinase which plays a crucial role in haemostasis and thrombosis. An abnormal activity or overexpression of this protein is associated with a variety of diseases. A great deal of attention was devoted to the construction of high-throughput biosensors for accurately detect thrombin for the early diagnosis and treatment of related diseases. Herein, we propose a new approach to modulate the interaction between α-thrombin and the aptamer TBA_{15}. To this end, TBA_{15} was chemically conjugated to two peptide sequences (TBA-G_3FIE-Ac and TBA-G_3EIF-Ac) corresponding to a short fragment of the acidic region of the human factor V, which is known to interact directly with exosite I. Surface Plasmon Resonance (SPR) results showed enhanced analytical performances of thrombin with TBA-G_3EIF-Ac than with TBA wild-type, reaching a limit of detection as low as 44.9 pM. Electrophoresis mobility shift assay (EMSA) corroborated the SPR results. Molecular dynamics (MD) simulations support experimental evidences and provided further insight into thrombin/TBA-peptide interaction. Our findings demonstrate that the combination of TBA_{15} with key interacting peptides offers good opportunities to produce sensitive devices for thrombin detection and potential candidates to block thrombin activity.

KEYWORDS: Thrombin, Biosensor, Binding affinity, Inhibition, Aptamer-peptide conjugate

1. Introduction

α-thrombin is a trypsin-like serine proteinase that plays a crucial role in haemostasis and thrombosis [1]. Since its discovery in the 19th century, α-thrombin has been extensively studied due to its complexity in function and regulation, since it acts paradoxically as pro-coagulant and as anti-coagulant factor [2]. α-thrombin is the product of an enzymatic amplification network, in which inactive components are activated by proteolytic cleavage [3-5]. A primary function of α-thrombin relies on the conversion of soluble fibrinogen into insoluble fibrin clot [6], that anchors platelets to the site of an injury initiating the repair process [7].

α-thrombin is composed by two polypeptide chains, chain A (36 residues) and chain B (259 residues), which are covalently linked through a disulfide bond. Chain B is organized in two adjacent β-barrels and contains the active site and two basic exosites, I and II [4]. The active site, with the reactive Ser195 residue at the base, is highly negatively charged and located in a deep canyon flanked by two loops, the 60-insertion and γ-loop. These two loops restrict the entrance to the active site helping to establish the substrate and inhibitors specificity. The exosite I is located to the right of the active site and is also known as fibrinogen recognition site. It contains hydrophobic patches and numerous charged residues. The location of these residues in the surface of exosite I provide electrostatics map-reading for the fibrinogen to the active site [8]. Exosite II is located opposite to exosite I and contains several charged residues, however does not include a hydrophobic area in the surface. Exosite II is prepared for the interaction with polyanionic ligands like glycosaminoglycan (GAG) and heparin [9, 10]. The natural substrates, cofactors and inhibitors compete for the three different sites of thrombin: the active site, exosite I and exosite II [2, 11, 12].

For these reasons, α-thrombin is an important protein target for anticoagulation and cardiovascular diseases therapy [3, 5]. Endogenous α-thrombin inhibitors are serpins AT and HCII, however they need specific interactions with glycosaminoglycans, like heparin, to become efficiently active [3, 10, 13]. Heparin in its full or truncated low molecular weight forms has been selected as the most relevant anti-coagulant drug for the prevention and treatment of thrombosis [14]. In addition, heparin binds to a large number of regulatory proteins within the complement system [15] and to different blood cells, for instance endothelial cells and monocytes [16]. Exogenous inhibitors come from diverse protein families and are normally found in the saliva of blood suckers as part of an anticoagulant mix that allows them to feed [17, 18].

In addition, single-stranded DNA oligonucleotides (ssDNA) that bind specific thrombin [19, 20] have been developed by selection of combinatorial libraries of oligonucleotides (SELEX) [21]. These ssDNAs molecules contained a 14–17 nt consensus sequence, with eight highly conserved guanine residues, which form a central core built of two guanine quartets. These oligonucleotides are known as α-thrombin binding aptamers (TBAs). Among the TBAs, the 15-mer with d(5′GGTTGGTGTGGTTGG3′)[19] sequence presents a strong anticoagulant activity at the nanomolar range [22]. Its interaction with the exosite I prevents α-thrombin to interact with fibrinogen and platelet aggregation [23, 24]. According to structural studies [25-27], TBA_{15}, in the presence of α-thrombin or specific cations such as K+ forms an unimolecular, antiparallel G-quadruplex with a chair-like conformation, consisting of two G-quartets connected by a single TGT loop and two TT loops.

Clinical trials have shown that this compound has interesting anticoagulant properties, however, its activity is too short because it is quickly degraded. A large number of derivatives

have been studied in order to increase the affinity to thrombin and/or its stability to nuclease degradation [12, 28]. In addition a modest antiproliferative activity has been found for TBA as a consequence of potential binding to nucleolin [29]. Recently, modified TBA derivatives with higher antiproliferative activity and lower anticoagulant properties have been described [30, 31].

In addition, TBA has been used for the construction of biosensors for the detection of thrombin [32] and it has been used as model compound for the optimization of aptasensors [33].

New approaches for the design of pharmaceutical agents against thrombin could possibly take into account the synergistic effect of polyvalent binder's. Herein, we design, synthesize and characterize for the first time the affinity of two α-thrombin binding aptamer conjugates that are covalently linked to a short peptide sequence corresponding to a fragment of the acidic region of the human factor V, which interact directly with α-thrombin exosite I [34]. This conjugation is expected to contribute positively to α-thrombin anchorage since both TBA and peptide have the ability to specifically bind to exosite I. Previous to this work oligonucleotides-peptide conjugates have been used as fluorescent probes, molecular tags [35] and cellular uptake enhancers [35, 36]. In particularly, a TBA-peptide conjugate was described for the visualization of K^+ ions in cells [37]. But this peptide was mainly used as scaffold for anchoring a biotine and a fluorescent probe to TBA. In our communication, the peptide is designed to interact with thrombin providing a synergetic anchoring of the aptamer. For inspecting the effect of TBA-peptide conjugation on binding affinity, experimental techniques such as Electrophoresis Mobility Shift Assay (EMSA) and Surface Plasmon Resonance (SPR) will be conducted. This latter methodology will allow us to follow in real-time the binding of thrombin on the TBA-peptide functionalized biosensor, while determining accurately the limit of detection for α-thrombin. In turn, EMSA assay permits to evaluate the propensity of TBA-peptide conjugates to interact with α-thrombin in solution.

Molecular dynamics (MD) will be used to determine the free energies of binding between α-thrombin and TBA-peptide conjugates. Information about the intermolecular interactions in the complexes will be also assessed.

2. Methods

2.1. Design of the TBA-peptide conjugates

The two crystals structures 1HAO [38] and the 3P6Z [34] containing α-thrombin bound to TBA or to the peptide (EIFEPPES) were used for the design of the conjugates. First, we selected just one of the two dimers described in the crystal structure 3P6Z. Then, the two α-thrombin molecules were superimposed using the molecular visualizer PyMOL. We extracted the TBA and the peptide coordinates to build up the connectivity between both molecules with the program Avogadro [39, 40]. Finally, the new coordinates were confirmed to verify whether TBA-peptide conjugates were located in exosite I.

2.2. Synthesis of modified TBAs

Modified TBAs were synthesized on several batches of 1-µmol scale (CPG) synthesis and the standard protocols [41]. The name and sequence of different modified TBAs are listed in Table **1**. The Amino-Modifier C_6 was site-specifically inserted into the TBA at the 5' end. During the addition of the amino linker we avoided the use of the capping step to prevent partial acetylation of the amino group in further chemical steps. Oligonucleotides for biosensing were prepared starting with the 3' end thiol modification and followed by 5' additional thymidines. The solid supports carrying the 5'-amino oligonucleotides were stored at -20 °C until further used.

2.3. Synthesis of TBA-peptide conjugate

Solid-phase peptide synthesis was performed manually in a batch procedure using N^{α}-Fmoc-protected amino acids. Syntheses were performed on 0.5-1 μmol scale. First, the support carrying the 5'-amino oligonucleotides were treated with a solution of 20% piperidine in DMF for 4 min to remove potentially reactive acetyl groups[42]. Next, the MMT group was removed using 3% TCA in DCM, neutralized with 5% DIPEA in DCM and washed in CH_3CN. The resulting support was treated with a mixture of Fmoc-amino acid (20 equiv), PyBOP (20 equiv) and DIPEA (40 equiv) in 0.2-0.3 ml of DMF for 5 hrs. Then, the solution was filtered and the support was washed with DMF and a second coupling of the same amino acid in the same conditions [Fmoc-amino acid (20 equiv), PyBOP (20 equiv) and DIPEA (40 equiv) in 0.2-0.3 ml of DMF] was performed over night. The glutamic acid couplings were performed with 20 equivalents of HATU instead of PyBOP. Next the resin was washed with CH_3CN three times and twice with DMF. The Fmoc group was then removed using a 20% piperidine solution in DMF for 5 min and the support was washed in CH_3CN and DMF. This process was repeated a second time. At the end of the synthesis the amino terminal was acetylated with a mixture of Ac_2O:DIPEA:DMF (0.1:0.17:1.53) to prevent the cyclation of the side chain of the glutamic acid.

2.4. Deprotection and purification of TBA-peptide conjugate

The side chain of the glutamic acid was deprotected with a 5% TCA solution in DCM for 1 hr, washed with CH_3CN and dried. Next the supports were treated with 32% aqueous ammonia at 55 °C for 1 hr or at room temperature overnight. Ammonia solutions were concentrated to dryness and the products were desalted over a NAP-10 column eluted with water. The resulting products were further purified by reversed-phase HPLC with 20 min linear gradient from 0 % to 30%,

flow rate 3 mL/min; solution A was 5% ACN in 0.1 M aqueous TEAA and B 70% ACN in 0.1 M aqueous TEAA. The length and homogeneity of the oligonucleotide-peptide conjugates were checked by MALDI-TOF (**Table 1**). The products concentration was determined by absorbance measurements (260 nm) and their extinction coefficient was considered as the TBA_{15}. These samples were kept dry at -20 °C until further use.

2.5. Melting Temperature studies and CD spectra

Melting curves of the TBA-peptide conjugates were measured by monitoring the absorbance hyperchromicity at 295 nm. The UV absorption spectra were recorded at 1°C/min intervals, with a 1 min equilibration time at each temperature value; the sample was heated over the range 20-80 ºC. Buffer solution was 10 mM sodium cacodylate pH 7.0 and 100 mM KCl. The concentration of the samples was around 1.66 μM. Each sample was allowed to equilibrate at the initial temperature for 5 min before the melting experiment was started. The melting temperatures (Tm) are the average value of a pair of Tm experiments.

Circular dichroism (CD) measurements were recorded at the same concentration and using the same buffer as for the denaturing curves. The spectra were registered at 15 °C over a range of 205–320 nm with a scanning speed of 100 nm/min, a response time of 4 s, a 0.5-nm data pitch, and a 1-nm bandwidth.

2.6. α-thrombin-binding assay

The interaction between TBA-peptide conjugates and α-thrombin were analyzed by gel electrophoresis. The TBAs-peptide conjugates (4 μM) were mixed with increasing concentrations of α-thrombin. The mixtures were left to interact for 1 hr at room temperature in

100 mM Tris pH 7.4, 50 mM AcOH, 2 mM KCl, 12.5 mM $Mg(OAc)_2$ and 5 mM EDTA. Complexes formation was analyzed on a 10% polyacrylamide gel at 80V, at 4 °C for 4 hrs in the same buffer.

2.7. SPR analysis of the TBA-peptide conjugates with α-thrombin

The interaction between α-thrombin and TBA-peptide conjugates was monitored and quantified by a home-made SPR [43]. Gold sensor chips were cleaned and prepared prior to experiments. Briefly, the gold chips were rinsed with pre heated solvents (i.e., trichloroethylene, acetone, ethanol, and dH_2O). Then, sensor chips were dried with N_2 flux and placed in a UV/O_3 generator (BioForce Nanosciences, USA) for 20 min. After that, gold sensor chips were subsequently rinsed with ethanol and water and dried under N_2 flux. The TBA peptide conjugates were immobilized with 100 mL of immobilization solutions (1 μM TBA-peptide in the following solution (20 mM Tris pH 7.4, 140 mM NaCl, 5 mM KCl, 1 mM $MgCl_2$) in the gold chips in a humid chamber O/N. Then, they were rinsed with DEPC-H_2O, dried with N_2, and placed in the sensor device. The interaction between oligonucleotide-peptide conjugates and α-thrombin was detected by flowing over the sensor different concentrations of α-thrombin in the same buffer conditions at a 16 μL/min constant rate and at room temperature (RT). Finally, the data were collected using Origin 8.0 software. The experimental detection limit (LOD) was defined as the target concentration giving a ΔR (%) in the hybridization signal at least three times higher than that of the standard deviation of a blank signal. The limit of quantification (LOQ) was defined as the target concentration giving a ΔR (%) in the hybridization signal at least ten times higher than that of the standard deviation of a blank signal.

2.8. MD simulations

2.8.1. Construction of solvated systems

Molecular dynamics (MD) simulations were performed to study the binding energies of human α-thrombin with TBA_{15} and peptide-modified TBA. We sought to understand the effect of conjugating the newly designed peptides to TBA on α-thrombin/TBA interaction by comparing the average binding energies obtained from a set of replicate simulations. Similarly to what consider in peptide design, the crystal structures obtained from RCSB PDB with IDs 1HAO [38] and 3P6Z [34] were used to define the initial coordinates for the complexes α-thrombin/TBA (system 1), α-thrombin/TBA-G_3FIE and α-thrombin/TBA-G_3EIF. The Leap module of AMBER14 was used to modify the sequence of the reference peptide detailed in PDB 3P6Z to match the ones tested experimentally. The aminohexyl linker was parameterized in the R.E.D.D. server [44] that automates the calculation of RESP charges at the HF/6-31G(d) level of theory, consistent with AMBER's ff14SB force field [45]. The lacking residues of human α-thrombin were modelled through the structural template-based atom fill-in tool Modeller9v15 [46]. The α-thrombin extremes were capped with neutral acetyl and N-methyl group, respectively. The overall charge of α-thrombin was set to correspond to pH=7.4. The initial conformations were minimized for 2500 cycles applying the steepest-descent algorithm in implicit Generalized Born (GB) solvent. The resulting geometries were then solvated using a TIP3P waters [47] in an octahedral water box with a 12 Å padding in all directions around the surface of complexes. The solvent molecules added were made to be identical within systems, to ensure their accurate energetic comparison. The sodium and chloride ions were added to the systems to reach a concentration of approximately 150 mM.

2.8.2. Molecular Dynamics simulations

Eight 50-ns MD simulations for each system were performed using AMBER's ff14SB force field. Replicate simulations were assigned with different initial velocities, to generate independent simulations. Hydrogen bonds were held fixed using the SHAKE algorithm [48] Short-range interactions were set to a cutoff of 10 Å and particle mesh Ewald (PME) [49] was applied for long-range electrostatics. Minimization, heating and equilibration stages were sequentially performed involving: (i) 1000 steps for the steepest-descent algorithm, followed by 1000 steps of conjugate-gradient algorithm, while 25 kcal mol^{-1} $Å^{-2}$ of positional restraints were imposed on α-thrombin/aptamers atoms; (ii) 2500 steps of both algorithms, steepest-descent and conjugate-gradient were applied to unrestrained systems; (iii) systems were heated from 0 to 298 K using Langevin thermostat over 1 ns with collision frequency of 2 ps^{-1} and 5 kcal mol^{-1} $Å^{-2}$ of positional restraints on thrombin/aptamers atoms; (iv) finally, systems were equilibrated at constant pressure and at 300 K for 2 ns using Langevin thermostat, and assigning 0.5 kcal mol^{-1} $Å^{-2}$ of positional restraints thrombin/aptamers atoms. For all stages the time step was set to 2 fs. MD runs were performed on Navigator computing cluster of LCA-UC [50] using the CPU version of PMEMD program in AMBER14 [51]. H-bond analysis were carried out in AMBER's Ptraj program and processed via an in-house script developed by the authors using Fortran 77 and R programming. The MD run that presented a value of free energy closer to the averaged free energy value was selected to conduct H-bond analyses. The distance between acceptor-donor was considered to be equal or less than 3.5 Å and the angle cut-off of equal or higher than 135°. The details of MM-GBSA analyses and the description of the method used for inspection of the intermolecular interaction are provided in Supplementary data.

3. Results and discussion

3.1. Design of the TBA-peptide conjugates

As starting point we analyzed two crystal structures of α-thrombin forming complex with TBA and a peptide derived from the human factor V from the RCSB protein data bank (PDB IDs 1HAO [38] and 3P6Z [34]). The pdb 1HAO is the structure of the complex between α-thrombin and TBA and the pdb 3P6Z contains a dimer of α-thrombin bound to the peptide with sequence EIFEPPES. After superimposing the two α-thrombin structures the binding region (exosite I) of the two ligands do not undergo significant conformational changes as a low RMSD value of 0.481 was obtained (Supplementary **Fig. 1**). The peptide residues, EPPES, were removed to avoid overlapping with TBA nucleotides, while the coordinates of the last residues EIF were preserved. Upon analyzing the binding site of the TBA and the peptide we could observe a close proximity between the 5' end of the TBA. Three glycine residues and a linker, aminohexyl, were introduced in peptide structure to allow the binding between 5' end of TBA and peptide. The effect of the amino-acid sequence in the interaction to thrombin was inspected by constructing peptides with inverted sequences EIF and FIE.

3.2. Synthesis, deprotection and purification of modified TBAs

We synthesized the TBA–peptide using standard DNA synthesis [41] and Fmoc-protected amino acids using a method developed in our laboratory [42]. Usually, the stepwise synthesis of oligonucleotide-peptide conjugates using the same support starts with the assembly of the peptide, as Boc-protected amino acids can be employed avoiding the use of acid treatment in the presence of the oligonucleotide chains. However, in this case, the peptide moiety is located at the 5' end of the oligonucleotide. For this reason, the TBA oligonucleotide was assembled first on

controlled pore glass (CPG) supports using standard 2-cyanoethyl phosphoramidites. After the completion of the TBA sequence, the N-6-MMT-aminohexyl-linker was incorporated to the 5' end of the DNA to generate an amino group for the assembly of the peptide. Following the coupling of the amino linker, the capping step was avoided to prevent undesired acetylation of the amino group as described [42]. Nevertheless, a washing step with piperidine was incorporated prior to the deprotection of the aminohexyl-linker to remove potentially reactive acetyl groups that may be produced in previous phosphoramidite coupling cycles [42].

Subsequently, the peptide sequences were assembled to the 5' end of the TBA to obtain the desired oligonucleotides conjugate. For the addition of the triglycine sequence we used the available Fmoc-triglycine derivative. To increase the incorporation efficiency of glutamic acid, the coupling reagent PyBOP was replaced by HATU. The 2-phenylisopropyl (PheiPr) group was selected for the protection of the side chain of glutamic acid. Other acid labile groups such as t-butyl ester were not adequate as the strong acid conditions needed for their removal can cause the depurination of the TBA oligonucleotide during the peptide deprotection step. In addition, we decided to acetylate the amino terminal end of the oligonucleotide-peptide conjugates before acid deprotection of the side chain of the glutamic acid in order to inhibit potential pyroglutamic formation and to increase the stability of the final product. The deprotection of the side chain of the glutamic acid was optimized by increasing the trichloroacetic acid solution percentage and the reaction time (5% and 1 hr). Finally, the treatment of the support with concentrated aqueous ammonia solution was used to deprotect the oligonucleotide moiety and liberate the conjugate from the solid support. The synthetic protocol is shown in **scheme 1**.

The resulting synthesis crudes were analyzed by HPLC giving a main product. These products were collected and characterized by MALDI-TOF presenting the expected mass, which are

shown in **Table 1**. The HPLC profiles of the products obtained are shown in **Fig. 1** and Supplementary **Fig. 2**.

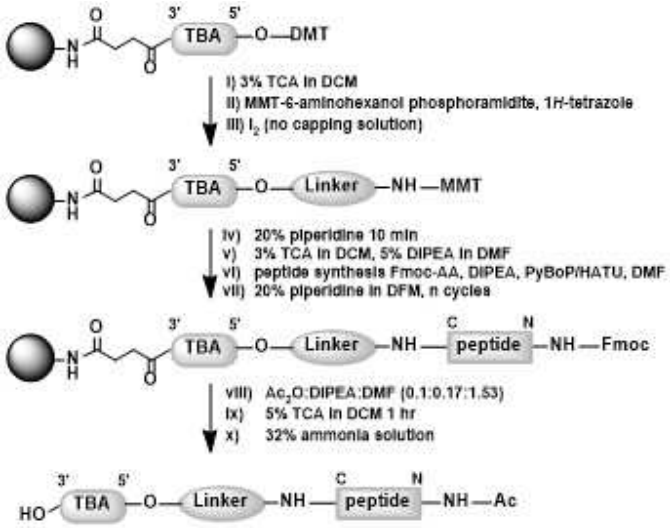

Scheme 1. Schematic representation of the process used in this work for the Solid-Phase Synthesis of Oligonucleotide-peptide conjugates including some small modifications to the previously described methodology [42]. Linker: phosphate-O-$(CH_2)_6$.

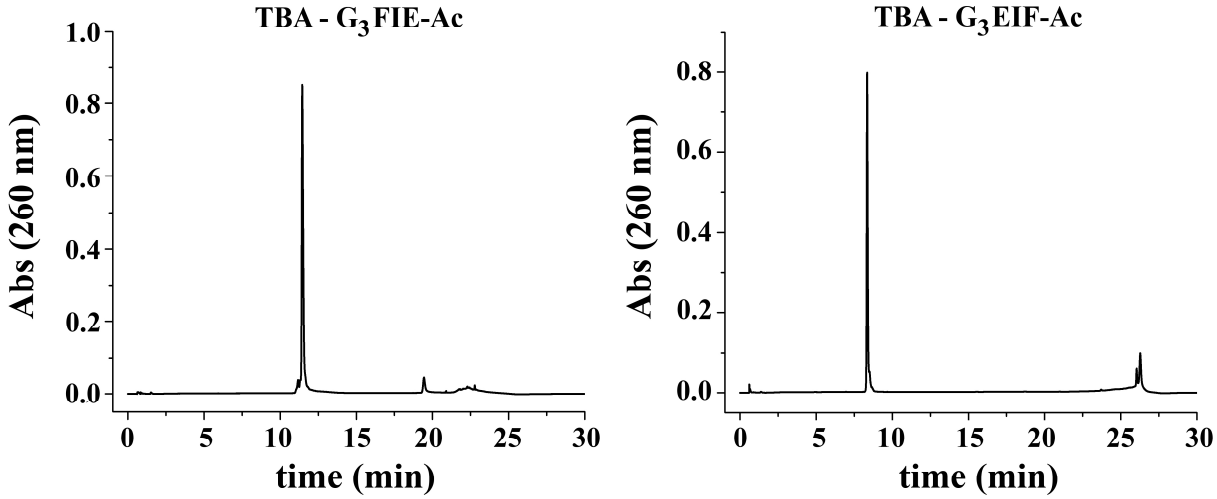

Fig. 1. HPLC analytical profiles of the different conjugate prepared in this work (XBridge OST C_{18} column).

Table 1. Sequence, melting temperature (T_m) and mass spectra of TBA-peptide conjugates prepared in this study.

Sample	Sequence (3'-5')	T_m (°C) [a]	ΔT_m	M_{calc} M_{found}
TBA	GGTTGGTGTGGTTGG	49.5	-	4725/4726
TBA-Ac	GGTTGGTGTGGTTGG-linker-Ac	40.2	-9.3	4946/4950
TBA-G_3FI	GGTTGGTGTGGTTGG-linker-G_3FI	40.8	-8.7	5377/5372
TBA-G_3EIF-Ac	GGTTGGTGTGGTTGG-linker-G_3EIF-Ac	35.1	-14.4	5506/5511
TBA-G_3FIE-Ac	GGTTGGTGTGGTTGG-linker-G_3FIE-Ac	39.1	-10.5	5506/5502
[b]R-S-S-T_5-TBA-G_3EIF-Ac 5⟶3	R-S-S-TTTTTGGTTGGTGTGGTTGG-linker-G_3EIF-Ac	n.d.	----	7273/7282
[b]R-S-S-T_5-TBA-G_3FIE-Ac 5⟶3	R-S-S-TTTTTGGTTGGTGTGGTTGG-linker-G_3FIE-Ac	n.d.	----	7273/7277

[a] 10 mM sodium cacodylate, 100 mM KCl pH 7.
[b] disulfide protected form. Uncertainty 0.5°C. n.d. not determined. Linker: O-phosphate-O-$(CH_2)_6$-NH.

3.3. Thermal denaturation studies and CD spectra

In order to analyze the effect of the incorporation of short peptide sequence at the 5' end of the TBA in the stability of the intramolecular antiparallel quadruplex structure, we have recorded the corresponding melting curves (Supplementary **Fig. 3**) allowing us to determine the melting temperatures (Tm), (see **Table 1**). A single transition was observed at 295 nm that corresponds to the denaturation of G-quadruplexes [52].

Unmodified TBA presents a Tm of 49.5 C and shows a CD spectrum with positive peaks at 295 and 245 nm as well as a negative peak at 265 nm. These features are in good agreement with those reported previously for antiparallel G-quadruplex [53, 54]. Surprisingly, the incorporation of the acetylated amino linker at the 5' end of the TBA produced a considerable decrease in the thermal stability of the TBA obtaining a Tm of 40.2 °C and it may be due to the presence of the phosphate group at the 5' end [55]. This reduction in thermal stability is maintained in one of the two peptide sequences and in its truncated version without the glutamic acid (TBA-G_3FIE-Ac and TBA-G_3FI).

However, the oligonucleotide-peptide conjugate TBA-G_3EIF-Ac presented a higher decrease in the stability of the quadruplex structure (ΔTm = -14.4 °C). The exchange of the two amino acids in the peptide sequence increase ΔT by ca. 4 °C. These results indicated that the incorporation of a phosphate group and a short peptide sequence at the 5' end has an influence in the stability of the G-quadruplex structure, which depends on the position of each amino acid in the sequence. Nevertheless, the CD spectra of the two modified TBA-peptides presented the typical features of an antiparallel G-quadruplex as TBA alone, indicating that the incorporation of the peptide sequence at the 5' end does not affect the overall structure as it is shown in **Fig. 2**.

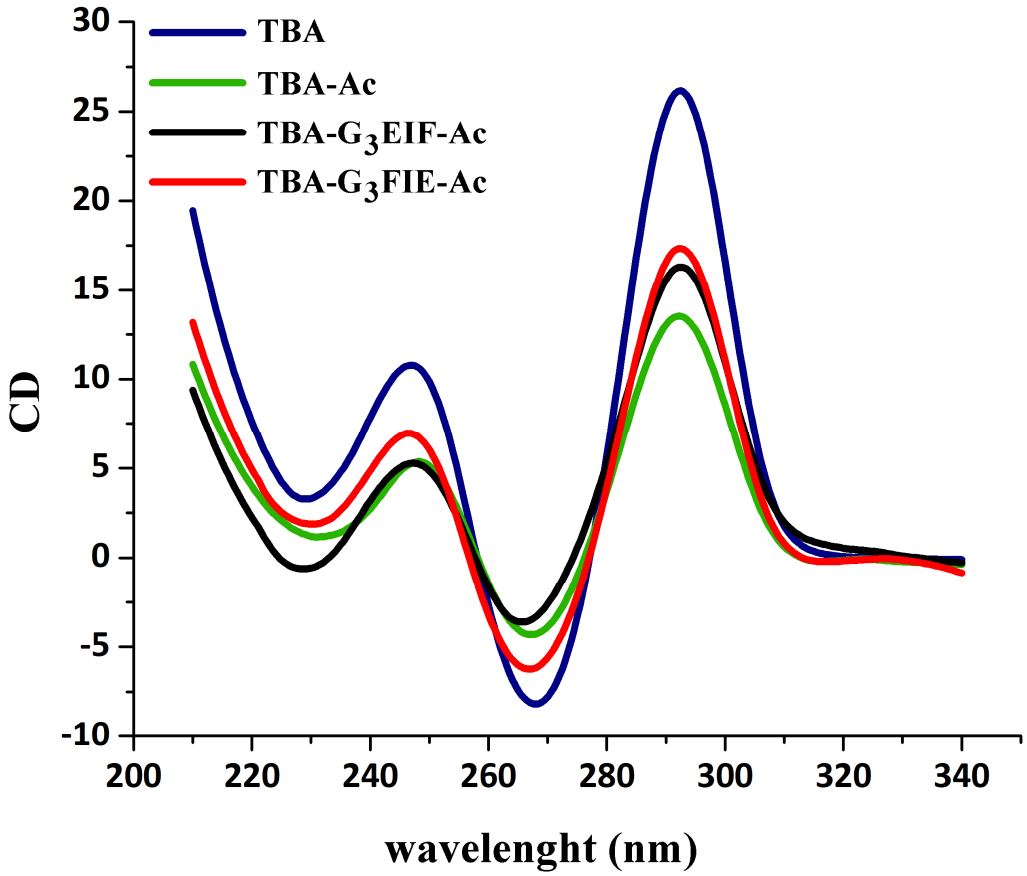

Fig. 2. CD spectra of the two oligonucleotide-peptide conjugates synthesized at 15 ºC compared with TBA-Ac and TBA alone.

3.4. α-thrombin-binding assay by EMSA

Next, we studied the complex formation between α-thrombin and the TBA-peptide conjugates (see **Table 1** for sequences) by electrophoresis mobility shift assay (EMSA). The amounts of TBA-complex formed at several TBA:Thrombin molar ratios are shown in **Fig. 3**. At all TBA: Thrombin molar ratios, the highest amount of thrombin complex was observed for TBA-G_3EIF-Ac followed by unmodified TBA and finally TBA-G_3FIE-Ac showed the lower affinity for α-thrombin. From these results and contrary to what could be expected from the decrease in G-quadruplex stability in the melting temperature experiments, we could conclude that the incorporation of a short peptide sequences at the end of the TBA does not disrupt its interaction with α-thrombin. These results are in agreement with others presented in the literature showing that α-thrombin binding is not dependent of the thermal stability of TBA modifications [30, 56]. Also, these results indicated that the affinity of the TBA for α-thrombin can be increased and modulated by the incorporation of a peptide sequence in the respective ends, and that the amino acids sequence orientation is an important factor for binding.

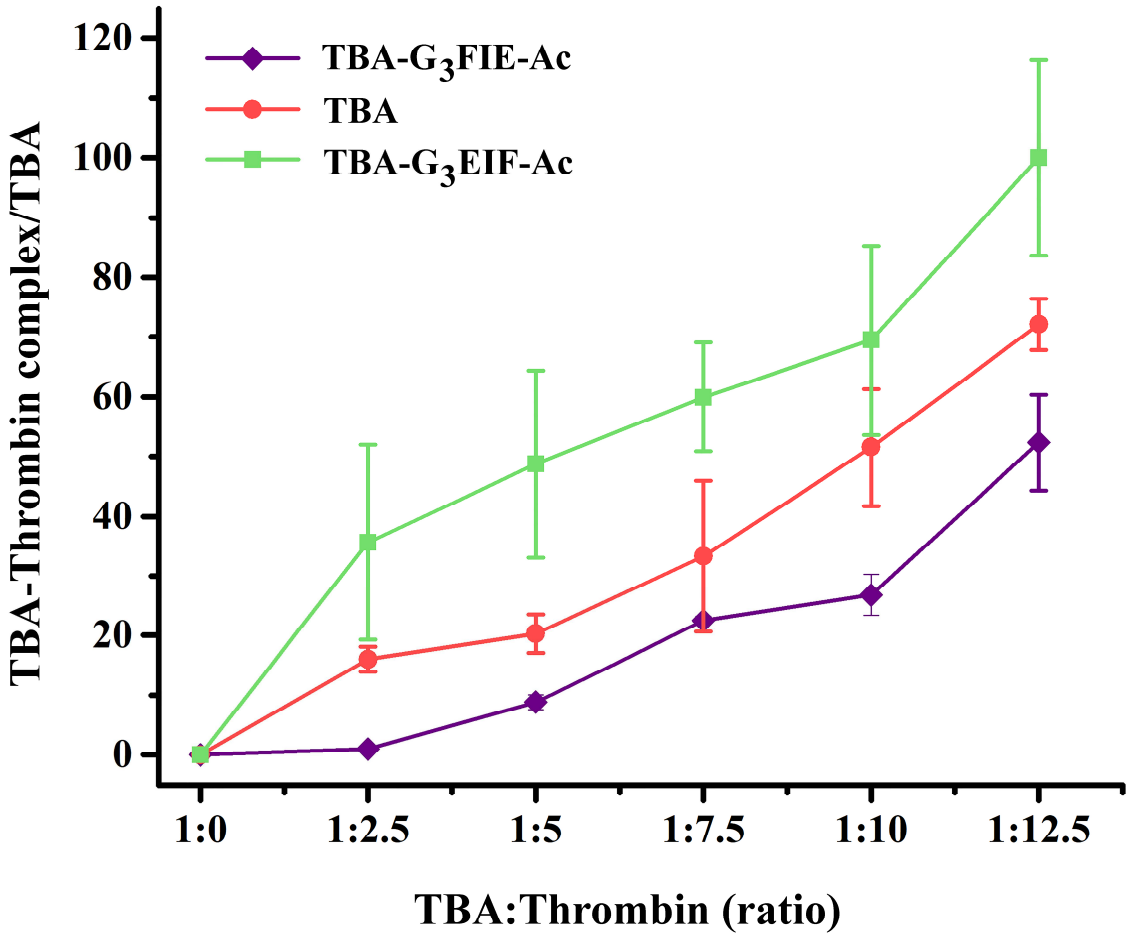

Fig. 3. EMSA assay of complexes between α-thrombin and TBA-peptide conjugates in 100 mM Tris pH 7.4, 50 mM AcOH, 2 mM KCl, 5 mM EDTA, 12.5 mM $Mg(OAc)_2$.

3.5. SPR analysis of the TBA-peptide conjugates with α-thrombin

SPR technology has been used to analyze thrombin interaction with different types of ligands [57, 58]. To prevent possible steric obstruction of the active site and of the exosite I of the protein, we decided to immobilize in the gold surface the unmodified and modified TBAs. For that purpose, we used TBAs modified with a thiol-group at the 3'-end, which will allow their attachment to the gold surface by chemisorption through thiol-gold chemistry. We included, also, a block of 5 thymidines nucleotides at the 3'-end as spacer in order to improve the formation of

the G-quadruplex structure and the accessibility of α-thrombin [59]. CD spectra confirm the antiparallel G-quadruplex structure of the thiolated oligonucleotides although the CD maxima are less intense than the unmodified TBA (data not show). The binding event is observed by alterations of the optical properties of the gold surface. Tiny variations in the refractive index produced by the interaction between TBA and α-thrombin changed the intensity of the reflected light, allowing real-time monitoring of the capture. We have studied the interaction of two peptide-TBA conjugates (TBA-G_3EIF-Ac and TBA-G_3FIE-Ac) with α-thrombin. For comparison purposes, we also assayed the complex interaction between the unmodified TBA with α-thrombin.

All results obtained with the three unmodified and modified TBA bioreceptors are show in **Fig. 4** and **Fig. S4**. We evaluated the interaction of the peptide-TBA conjugates with a range of α-thrombin concentrations. Triplicate measurements and calibration curves of each interaction were obtained and are represented in **Fig. 4**. The limits of detection (LOD) and quantification (LOQ) for each bioreceptor were calculated.

When comparing the obtained SPR curves, results show a clear difference in the performances of the modified surfaces for the detection of the α-thrombin analyte. The surface Gold-S-T_5-TBA-G_3FIE-Ac showed the lowest affinity to interact with α-thrombin, having a limit of detection of 124.33 pM and R^2=0.71 remarkably lower than the one calculated for TBA (49.12 pM, R^2=0.93). On the other hand, the biosensor with a surface functionalized with the Gold-S-T_5-TBA-G_3EIF-Ac displays enhanced analytical performances for α-thrombin in comparison with the latter one, reaching a LOD of 44.9 pM with R^2=0.99. As expected, the values calculated for the limit of quantification follow the same trend as LOD. The values obtained for LOD are in agreement with those reported in literature for aptasensors [60, 61], in the order of sub

nanomolar discarding the SPR biosensors that enhance their sensitivity by means of amplification procedures or by exploiting the properties of nanoparticles [62].

The higher sensitivity detected for surfaces functionalized with Gold-S-T_5-TBA-G_3EIF-Ac corroborates the data obtained from electrophoresis experiments. From these experiments, it is clear that by conjugating a peptide moiety derived from human factor V with TBA, the affinity of the aptamer for thrombin can be modulated, revealing an useful approach to build better biosensors for thrombin detection.

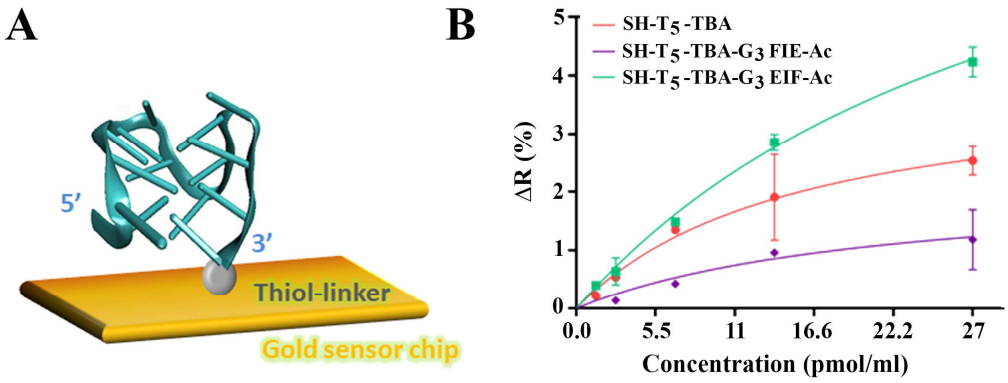

C

Receptor	TBA	TBA-G_3EIF-Ac	TBA-G_3FIE-Ac
LOD (pM)	49	45	120
LOQ (pM)	160	150	430
K_d (nM)	15	15	18

Fig. 4. SPR measurements of the TBA-peptide conjugates with α-thrombin. In panel A, schematic representation of the gold sensor chip functionalization with TBA as a receptor through a thiol-linker. In panel B, SPR curves of the detection of the interaction between α-thrombin with TBA or with the two TBA-peptide conjugates variant in 20 mM Tris pH 7.4, 140 mM NaCl, 5 mM KCl, 1 mM $MgCl_2$. All data show mean value ±SD from the SPR-equilibrium signal of three measurements. In panel C are indicated the limits of detection (LOD) and the limit of quantification (LOQ) calculated for each receptor.

3.6. MD simulations

MD simulations have proven valuable in determining the thermodynamic properties of protein/ligand complexes in atomic detail, endowing a powerful predictive complement to experiments [63, 64]. We sought to compare the binding affinities of the complexes tested experimentally whilst gaining further insight regarding the sources dominating in thrombin and modified TBAs interaction. As mentioned above, the crystal structures 1HAO and 3P6Z were used to establish the initial positions of protein, peptides and aptamer, and different start velocities were imposed on simulation replicates to enhance sampling. In all the simulation runs, complexes rapidly reached equilibrium and show low RMSD oscillations in the last nanoseconds of simulation (Supplementary **Fig. 5**). In comparison, the RMSD variance range of the TBA conjugated to peptides is wider than the one of wild-type, suggesting that the presence of peptide induces larger conformational changes upon binding. In addition, the RMSF plot displays similar atomic fluctuation patterns for the thrombin bound to TBA and thrombin bound to modified-TBA which in general fluctuate < 1 Å (Supplementary **Fig. 6**). An exception occurs only for the γ-loop displaying higher atomic fluctuation especially when having TBA-G_3FIE-Ac.

For determining the thermodynamic properties involved in the interaction of α-thrombin and the set of aptamers tested experimentally the binding free energies were assessed by MM-GBSA methodology. This methodology is a popular method to estimate absolute free energies of protein-ligand complexes with a moderate computational effort [65, 66]. The average absolute binding free energy estimates are compared in **Fig. 5A**. The specific values for each replicate as well as the decomposed energies into the various items from electrostatics, Van der Waals, non-polar solvation and electrostatic solvation interactions are listed in supplementary **Table 1**. By comparing the average binding energy for wild type and modified-TBAs, results confirmed the

experimental observations. In particular, the conjugation of TBA with G_3EIF-Ac clearly enhances the interaction of α-thrombin/TBA (ΔG_{bind}= -26.1±3.9 kcal mol^{-1} for thrombin/TBA and ΔG_{bind} = -44.2±8.0 kcal mol^{-1} for thrombin/TBA-G_3EIF-Ac) while the conjugation with the parent G_3FIE-Ac peptide weaken the α-thrombin/TBA interaction (ΔG_{bind} = -20.8±5.9 kcal mol^{-1}). The value of absolute binding free energies estimated for α-thrombin/TBA is larger than those reported experimentally, which are comprised between -8 and -10 kcal mol^{-1}, calculated through different techniques [67-70]. It is well-known that the MM-GBSA method neglects the entropy loss associated with bound water molecules in a protein-ligand complex, but nevertheless this methodology provides a useful tool to compare related complex systems. The present results show that the trend found computationally is in good agreement with results obtained with EMSA and SPR assays.

In general, the decomposition of the binding free energy into different energy items highlights the relevant contribution of nonpolar and hydrophobic interactions ($\Delta G_{nonpol} = \Delta E_{vdw} + \Delta G_{SA}$) to binding free energies. Despite being unfavorable, the electrostatic contribution is more pronounced in thrombin/TBA-G_3EIF-Ac complex, since ΔG_{pol} become less positive. When binding free energies are decomposed into individual residues (see **Fig. 5B**), the results show differences between systems. For the wild-type TBA, the most contributive residues are the nucleotides located on the TT loops, 3, 4, 12 and 13 that are in close vicinity to α-thrombin exosite I. The conjugation of peptides to the TBA preserves the same profiles of interaction but reduces slightly the affinity of dT13, and for TBA-G_3FIE-Ac the interaction with dT14 is also reduced.

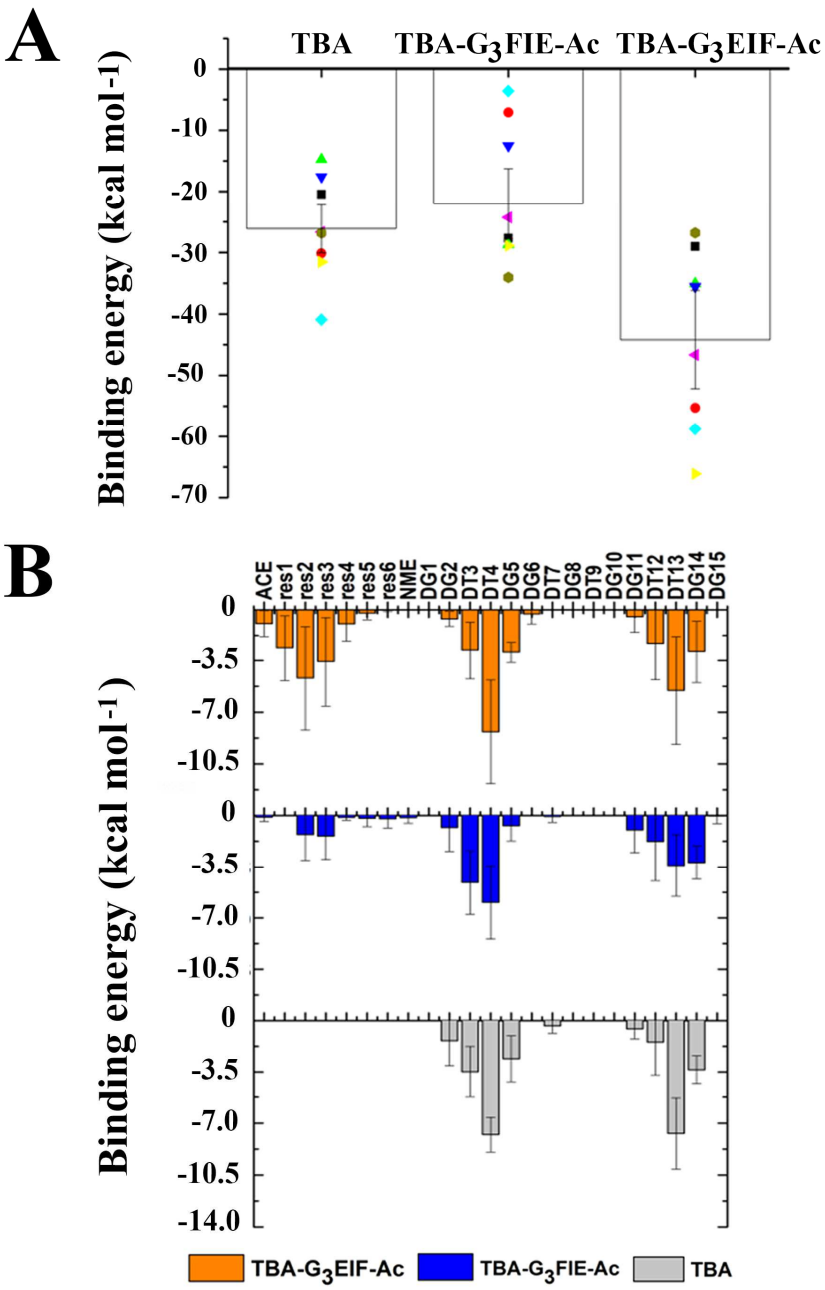

Fig. 5. MM-GBSA binding energy results for the α-thrombin/TBA, α-thrombin/TBA-G_3FIE-Ac and α-thrombin/TBA-G_3EIF-Ac simulation sets. The absolute binding energy values obtained for the 8 independent simulations are distinguished by different colored symbols while the bar indicates the overall mean value. All the data are given in kcal mol^{-1}, and the specific values for each replicate and average are provided in supporting information **Table S1**. Error bars represent the standard error of the mean (SEM) calculated for the 8 replicates.

Furthermore, the residues of G_3FIE-Ac peptide present low affinity to the thrombin residues being the isoleucine (I) and phenylalanine (F) the most prominent for the binding (>1 kcal mol^{-1}). For TBA-G_3EIF-Ac the triad E, I and F, in this order, make significant contributions to the binding affinity. The hydrogen bond analysis, depicted in **Fig. 6A**, detected four stable H-bonds not discarding ionic bonds between the amide groups of Arg75 and Tyr76 and the carbonyl groups of dT14 and dT13, while other contacts are established with protein residue Arg77A and the TBA nucleotides dT13 and dT14, as detected also in crystal structure [54, 71, 72]. The conjugation of G_3FIE-Ac peptide displays H-bonds with a dynamic occupancy, and just two prevalent H-bonds, where one is established between the glutamic acid (E) and Arg73 (**Fig. 6B**). In turn, TBA-G_3EIF presents several long time H-bonds formed not only between thrombin/TBA and thrombin/peptide but also within peptide/TBA (**Fig. 6C**). In this case, the peptide is buried in thrombin tertiary structure reaching inner residues such as Gln29 and Leu31, moving away from the initial position provided by the crystal structure.

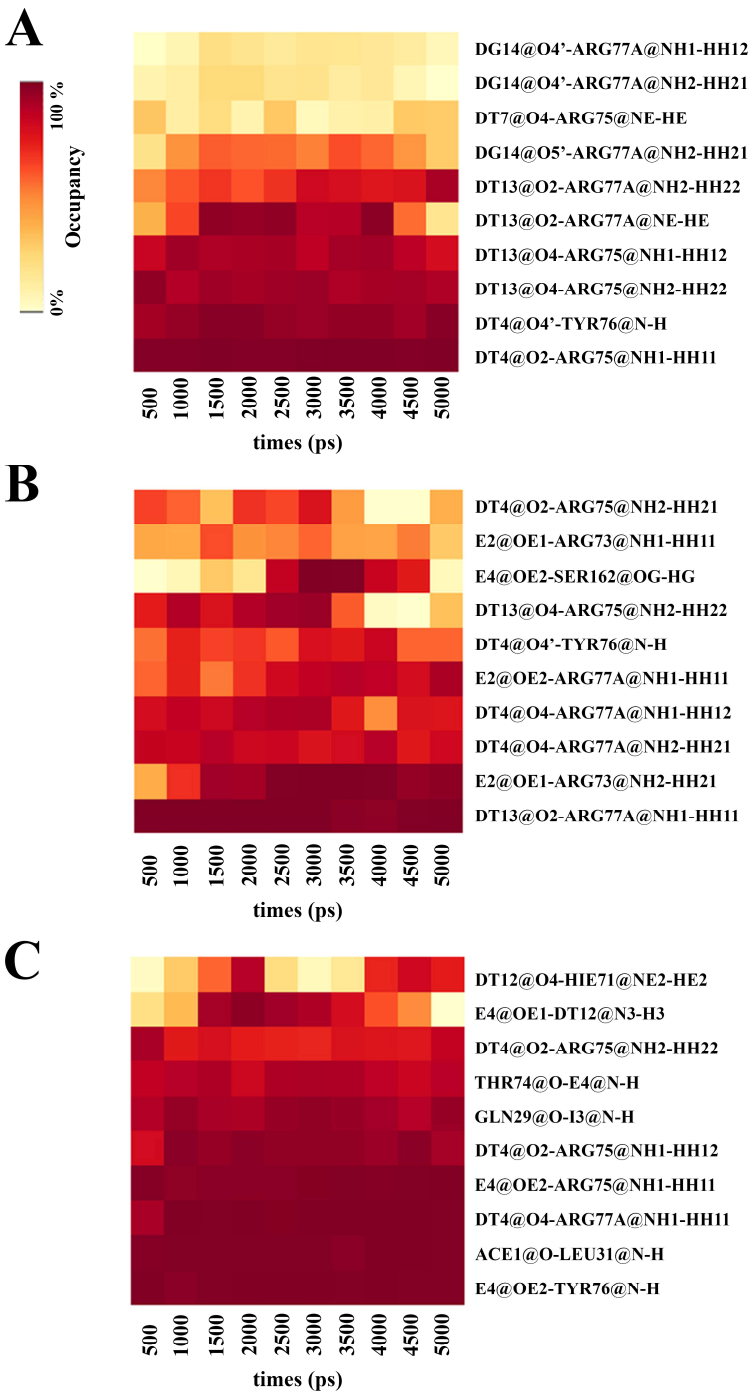

Fig. 6. Interaction between α-thrombin/TBA, α-thrombin/TBA-G_3FIE-Ac and α-thrombin/TBA-G_3EIF-Ac. In the panels are represented the occupancies of the most prominent hydrogen bonds formed between α-thrombin and a) TBA_{15}, b) TBA-G_3FIE-Ac and c)TBA-G_3EIF-Ac. Data represented correspond to the last 11 ns of MD simulation.

In addition, for a detailed description of intermolecular interactions, the binding patterns within the ternary systems thrombin/TBA-peptide are analyzed based on the topological features of the electronic charge densities, in order to decouple the types of interaction and rationalize the respective strengths. In **Fig. 7** and **8** the volume of the interacting regions allows inferring on the extent of the interactions within the thrombin/TBA-peptide conjugates. Binding specificity is suggested by discrete regions of enhanced interactions represented by the 3D isosurfaces. This specificity depends, as expected, on the nature of the protein residues involved in the interaction. Blue and red denote, respectively, stronger stabilizing/destabilizing interactions, while green indicates weak van der Waals-type interactions. Also included, are the respective 2D scatter plots, in which the asymmetry of the peaks reflects the favourable nature of the protein/ligand interactions. The peaks on the negative, stabilizing side of the plot are more intense than the corresponding peaks on the positive, destabilizing side, indicating that the balance of noncovalent forces in each binding scenario are in overall favouring the complex formation and stability.

A clear difference between both thrombin/TBA and thrombin/TBA-G_3FIE-Ac and thrombin/TBA-G_3EIF-Ac is observed in **Fig. 7** (panels A and B) and (panel A and C) respectively. The stability of the former interactions is essentially governed by several N-H···O hydrogen-bonds (represented by large volumes with blue centers), as also observed in **Fig. 6**. These hydrogen-bonds are identified by large diffuse peaks (ca. 5 N-H···O hydrogen-bonds in thrombin/TBA and 5 N-H···O and 1 N-H···O hydrogen-bonds in thrombin/TBA-G_3FIE-Ac), with the respective maximums defined at $-0.05 < \text{sign}(\lambda_2)\rho < -0.02$. In thrombin/TBA-$G_3$EIF-Ac (panel c), the type of hydrogen-bonds is similar, although the double $(N\text{-}H)_2\cdots O$ involving ARG75(N-H)-DT4(O) is more pronounced.

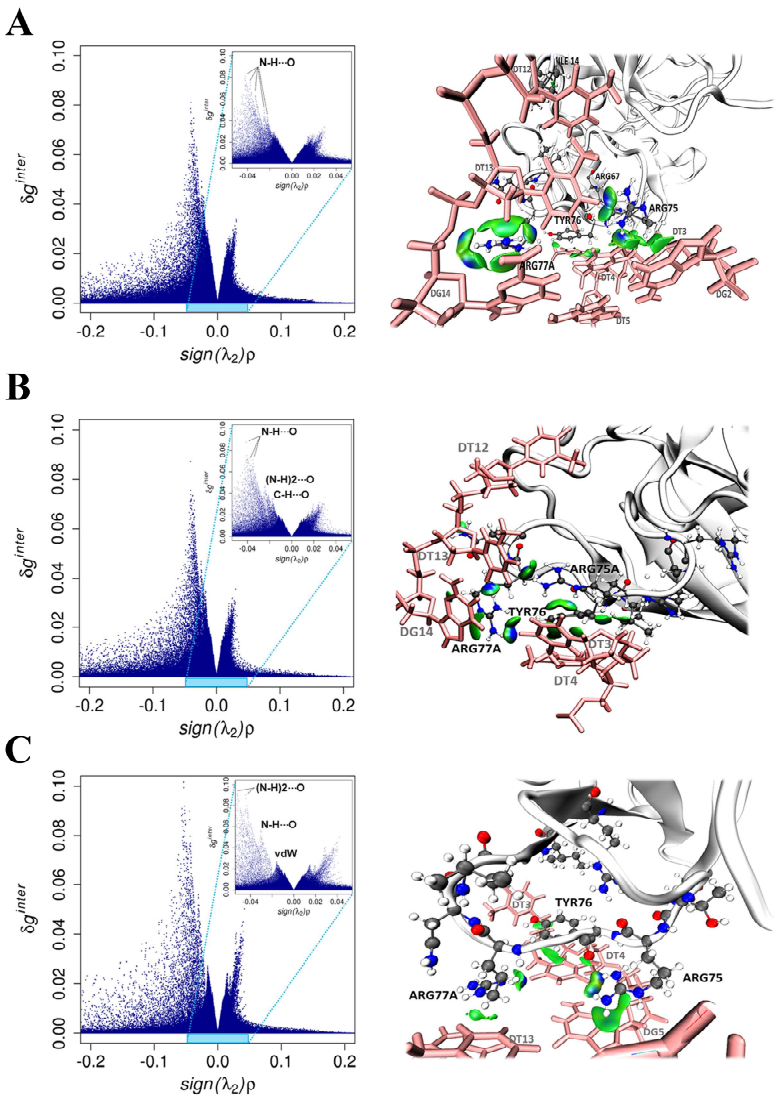

Fig. 7. Interaction patterns underlying the complexes between α-thrombin and (A) TBA, (B) TBA-G$_3$FIE-Ac, and (C) TBA-G$_3$EIF-Ac, represented in the 2D scatter plots (left) and IGMPlot isosurfaces (right). The structures of the complexes correspond to the last snapshot of 50 ns MD simulation. Isosurfaces show the total IGM interaction points for $\delta g^{inter} \leq 0.1$ and in the region $-0.2 \leq \text{sign}(\lambda_2)\rho \leq 0.2$. and are colored based on a blue-green-red scheme over the electron density range $-0.04 < \text{sign}(\lambda_2)\rho < 0.04$ a.u. Stabilizing/destabilizing noncovalent interactions are thus represented in blue/red and van der Waals forces are colored in green. Thrombin side chains are represented in white as cartoon while some relevant amino acids are featured in ball-and-stick, where carbon atoms are colored in grey, nitrogen in blue, oxygen in red and hydrogen in white.

These stronger hydrogen bonds are identified as the larger diffuse peaks at sign(λ2)ρ ≈ -0.054 and sign(λ_2)ρ ≈ -0.05, respectively, in the corresponding 2D scatter plot. There is also a third well-defined peak corresponding to the ARG77A(N-H)-DT4(O). In addition to the N-H···O hydrogen-bonds derived from the ARG75(N-H)-DT4(O) and also ARG774(N-H)-DT4(O) the thrombin-TBA-G_3EIF binding is also stabilized by slightly enhanced van der Waals interactions (corresponding to the flat green regions), established between ARG75 and DG5, ARG77A and DT13 and TYR76 and DT3-DT4 rings. In contrast to thrombin/TBA (panel A) and thrombin/TBA-G_3FIE-Ac (panel B), these weakly stabilizing van der Waals-type interactions are represented by the solid peak at sign(λ2)ρ ≈ -0.02. Such weak attractive forces have been recognized as important driving forces in the binding process of similar systems involving proteins and aptamers [38].

From **Fig. 8** (panels A and B), it is observed that the van der Waals interactions are almost comparable when the binding of protein/peptide-G_3EIF-Ac and protein/peptide-G_3FIE-Ac are considered. However, the number and nature of the hydrogen-bonds differ. In protein/peptide-G_3FIE-Ac (panel A) two N-H···O hydrogen bonds are established between ARG77A(N-H) and the carboxylic group of glutamic acid. The latter is also involved in one O-H···O hydrogen bond with the SER162 (O-H) moiety. These interactions can be identified in the more intense peaks on the left, at sign(λ_2)ρ ≈ −0.05 and sign(λ_2)ρ ≈ −0.03, respectively. The protein/peptide-G_3EIF-Ac binding (panel B) is favoured by four N-H···O hydrogen bonds established between LEU31(N-H)-ACE(O), I(N-H)-GLN29(O), and two ARG75(N-H)-E(O) and TYR86(N-H)-E(O). The triad ACE, F and I establish a network of stabilizing van der Waals interactions with neighbour protein residues. This extensive number of attractive interactions between G_3EIF-Ac and thrombin justifies the high affinity detected in MM-GBSA calculations. Comparing the

interactions promoted by both peptides, we may hypothesize that G_3FIE-Ac competes with TBA to interact with thrombin's exosite I, while G_3EIF-Ac shows the ability to interact with residues present in a distant region from exosite I, thus providing an additional interaction site, without disturbing the interaction between thrombin/TBA. Other peptides have demonstrated high affinity of phenylalanine to thrombin residues located in regions comprised within 31-35 residues [73, 74], providing useful insights for the design of high-affinity peptides.

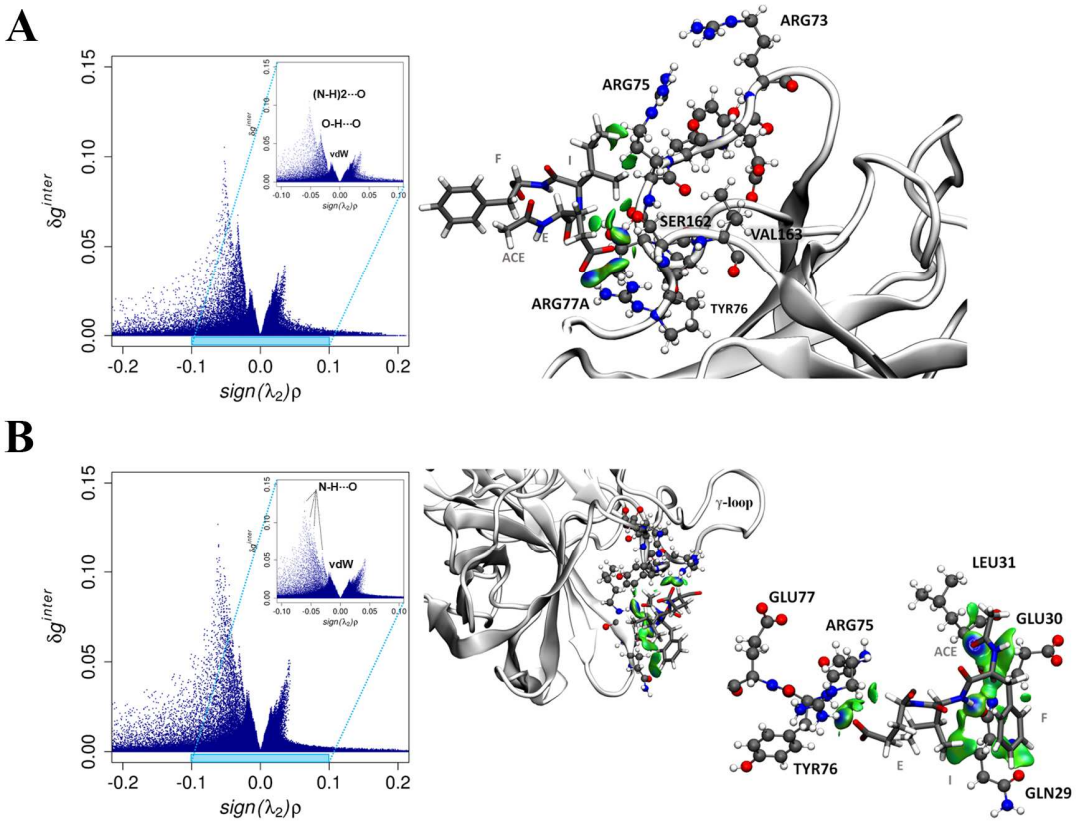

Fig. 8. IGMPlot isosurfaces illustrating the existent intermolecular interactions established between A) thrombin and G_3FIE-Ac and B) thrombin and G_3EIF-Ac. Stabilizing/destabilizing noncovalent interactions are represented in blue/red and van der Waals forces are colored in green (volume cutoff of δg^{inter}=0.15; color coding: $-0.1 \leq sign(\lambda_2)\rho \leq 0.1$). α-thrombin side chains are represented in white as cartoon while some relevant amino acids are featured in ball-and-stick, where carbon atoms are colored in grey, nitrogen in blue, oxygen in red and hydrogen in white. Peptides G_3EIF-Ac and G_3FIE-Ac are represented in thin lines.

4. Conclusion

Similarly to antibodies, DNA aptamers are widely used in biosensors and in the production of targeted therapies but offer several advantages including straightforward chemical synthesis, small size, lack of immunogenicity and possibility of chemical modification. Backbone and nucleobase modifications are the most commonly used strategies to increase nuclease resistance and/or to increase the affinity to the target [12]. In this work we described a new approach for the design of α-thrombin high-affinity conjugates, taking into account the synergistic effect that could arise from the combination of more than one binder. As demonstrated both experimentally and computationally, the covalent binding of TBA with a short peptide sequence, derived from the acidic region of human factor V which interacts directly with the exosite I, increases the TBA's affinity to the target α-thrombin protein. During the characterization, we have seen that this conjugate preserves the typical structural features of an antiparallel G-quadruplex, as the natural TBA. The free energies determined by MM-GBSA method reproduce the experimental evidences obtained in both EMSA and SPR methods. In particular, coupling the peptide G_3EIF-Ac guaranteed higher binding affinities than the cognate G_3FIE-Ac or the TBA alone. An accurate evaluation of intermolecular interactions within the complex demonstrated that G_3EIF-Ac promote H-bonds with thrombin residues not located in exosite I and also exhibit interactions with TBA. On the other hand, the reverse G_3FIE-Ac seems to compete with TBA for the same thrombin region. Therefore, the amino acid sequence seems to be determinant for the reinforcement of thrombin/TBA-G_3EIF-Ac interaction. The results described in the present work encourage the development of new oligonucleotide-peptides conjugates with potential to increase the affinity to target α-thrombin. In addition, this strategy is compatible with existing backbone and nucleobase modifications.

Funding

Spanish Ministerio de Ciencia e Innovación [Projects CTQ2010-20541, CTQ2014-52588-R, CTQ2017-84415-R]; CERCA Programme/Generalitat de Catalunya (2009/SGR/208); CIBER-BBN. The authors thank ICTS NANBIOSIS Biodeposition and Biodetection unit (U4) and oligonucleotide synthesis platform (U29) from CIBER-BBN. ICN2 is supported by the Severo Ochoa program from Spanish MINECO (Grant No. SEV-2017-0706); and Fundação para a Ciência e Tecnologia [SFRH/BPD/104544/2014 to A.F.J., SFRH/BD/95459/2013 to T.F.G.G.C., Nº 007630 UID/QUI/00313/2013 co-funded by COMPETE2020-UE]. Funding for open access charge: Spanish Ministerio de Ciencia e Innovación.

Author contribution

R.E. and C.F. conceived, designed, and supervised the project; A.A. and C.F. performed the synthesis and characterization of the TBA-peptides conjugates, A.A., L.M.L. and C.S.H performed and analyzed the SPR experiments, A.F.J., T.F.G.G.C. and A.C.C.P. performed and analyzed the MD simulations.

All authors have given approval to the final version of the manuscript.

The authors declare no competing financial interest.

Acknowledgment

The authors acknowledge the Laboratory for Advanced Computing at the University of Coimbra for providing {HPC, computing, consulting} resources that have contributed to the research results reported within this paper (URL http://www.lca.uc.pt). CIBER-BBN is an initiative funded by the VI National R + D + I Plan 2008-2011, Iniciativa Ingenio 2010, Consolider

Program; The Instituto de Salud Carlos III with assistance from the European Regional Development and NANBIOSIS.

Appendix A. Supplementary data

Reagents, instrumentation, MM-GBSA analyses, analysis and visualization of noncovalent interactions, superposition of the two crystal structures (supplementary **Figure. 1**), HPLC analytical profiles (supplementary **Figure. 2**), Melting temperatures profile (supplementary **Figure. 3**), SPR raw data (supplementary Fig. 4), Structural variations for the three simulation systems obtained MD simulations (supplementary **Figure. 5**), Root-mean-square-fluctuation (RMSF) (supplementary **Figure. 6**). Binding free energy calculated by MM-GBSA methodology (supplementary **Table 1**).

Abbreviations

DCM: dichloromethane; CPG: controlled pore glass; DIPEA: diisopropylethylamine; DMF: *N*,*N*-dimethylformamide; Fmoc: 9-fluorenylmethoxycarbonyl; LV200: polystyrene support (low volume); MMT: monomethoxytrityl; PyBOP: Benzotriazole-1-yl-oxy-tris-pyrrolidino-phosphonium hexafluorophosphate; PhiPr: 2-phenylisopropyl ester; O.D. optical units; TEAA: triethylammonium acetate; TCA trichloroacetic acid.

References

[1] E. Di Cera, M.J. Page, A. Bah, L.A. Bush-Pelc, L.C. Garvey, Thrombin allostery, Phys. chem. chem. phys. 9 (2007) 1291-1306.
[2] E. Di Cera, Thrombin, Mol. Asp. Med. 29 (2008) 203-254.
[3] J.A. Huntington, T.P. Baglin, Targeting thrombin--rational drug design from natural mechanisms, Trends in pharmacol. Sci. 24 (2003) 589-595.

[4] W. Bode, Structure and interaction modes of thrombin, Blood cells Mol. Dis. 36 (2006) 122-130.
[5] J.A. Huntington, Molecular recognition mechanisms of thrombin, J. Thrombos. Haemostas. 3 (2005) 1861-1872.
[6] A.S. Wolberg, Thrombin generation and fibrin clot structure, Blood Rev. 21 (2007) 131-142.
[7] T. Myles, T.H. Yun, L.L. Leung, Structural requirements for the activation of human factor VIII by thrombin, Blood 100 (2002) 2820-2826.
[8] I. Pechik, J. Madrazo, M.W. Mosesson, I. Hernandez, G.L. Gilliland, L. Medved, Crystal structure of the complex between thrombin and the central "E" region of fibrin, Proc. Natl. Acad. Sci. U.S.A. 101 (2004) 2718-2723.
[9] W.J. Carter, E. Cama, J.A. Huntington, Crystal structure of thrombin bound to heparin, J. Biol. Chem. 280 (2005) 2745-2749.
[10] W. Li, D.J. Johnson, C.T. Esmon, J.A. Huntington, Structure of the antithrombin-thrombin-heparin ternary complex reveals the antithrombotic mechanism of heparin, Nat. Struct.Mol. Biol. 11 (2004) 857-862.
[11] E. Di Cera, Thrombin interactions, Chest 124 (2003) 11S-17S.
[12] A. Aviñó, C. Fàbrega, M. Tintoré, R. Eritja, Thrombin binding aptamer, more than a simple aptamer: chemically modified derivatives and biomedical applications, Curr. Pharm. Des. 18 (2012) 2036-2047.
[13] J.A. Huntington, Mechanisms of glycosaminoglycan activation of the serpins in hemostasis, J. Thrombos. Haemostas. 1 (2003) 1535-1549.
[14] J.I. Weitz, Low-molecular-weight heparins, N. Engl. J.Med. 337 (1997) 688-698.
[15] H. Yu, E.M. Munoz, R.E. Edens, R.J. Linhardt, Kinetic studies on the interactions of heparin and complement proteins using surface plasmon resonance, Biochim. Biophys. Acta, 1726 (2005) 168-176.
[16] G.M. Arepally, Heparin-induced thrombocytopenia, Blood 129 (2017) 2864-2872.
[17] J.A. Huntington, Natural inhibitors of thrombin, Thromb. Haemost. 112 (2014) 583-589.
[18] C.Y. Koh, R.M. Kini, Thrombin inhibitors from haematophagous animals, Toxins and Hemostasis, Springer, 2010, pp. 239-254.
[19] R.F. Macaya, P. Schultze, F.W. Smith, J.A. Roe, J. Feigon, Thrombin-binding DNA aptamer forms a unimolecular quadruplex structure in solution, Proc. Natl. Acad.Sci. U. S. A. 90 (1993) 3745-3749.
[20] D.M. Tasset, M.F. Kubik, W. Steiner, Oligonucleotide inhibitors of human thrombin that bind distinct epitopes, J. Mol. Biol. 272 (1997) 688-698.
[21] L.C. Bock, L.C. Griffin, J.A. Latham, E.H. Vermaas, J.J. Toole, Selection of single-stranded DNA molecules that bind and inhibit human thrombin, Nature 355 (1992) 564-566.
[22] Q. Wu, M. Tsiang, J.E. Sadler, Localization of the single-stranded DNA binding site in the thrombin anion-binding exosite, J. Biol. Chem. 267 (1992) 24408-24412.
[23] W.X. Li, A.V. Kaplan, G.W. Grant, J.J. Toole, L.L. Leung, A novel nucleotide-based thrombin inhibitor inhibits clot-bound thrombin and reduces arterial platelet thrombus formation, Blood 83 (1994) 677-682.
[24] L.R. Paborsky, S.N. McCurdy, L.C. Griffin, J.J. Toole, L.L. Leung, The single-stranded DNA aptamer-binding site of human thrombin, J. Biol. Chem. 268 (1993) 20808-20811.
[25] K. Padmanabhan, K.P. Padmanabhan, J.D. Ferrara, J.E. Sadler, A. Tulinsky, The structure of alpha-thrombin inhibited by a 15-mer single-stranded DNA aptamer, J. Biol. Chem. 268 (1993) 17651-17654.

[26] J.A. Kelly, J. Feigon, T.O. Yeates, Reconciliation of the X-ray and NMR structures of the thrombin-binding aptamer d(GGTTGGTGTGGTTGG), J. Mol. Biol. 256 (1996) 417-422.
[27] K.Y. Wang, S.H. Krawczyk, N. Bischofberger, S. Swaminathan, P.H. Bolton, The tertiary structure of a DNA aptamer which binds to and inhibits thrombin determines activity, Biochemistry 32 (1993) 11285-11292.
[28] V. Esposito, M. Scuotto, A. Capuozzo, R. Santamaria, M. Varra, L. Mayol, A. Virgilio, A. Galeone, A straightforward modification in the thrombin binding aptamer improving the stability, affinity to thrombin and nuclease resistance, Org. Biomol. Chem. 12 (2014) 8840-8843.
[29] V. Dapic, V. Abdomerovic, R. Marrington, J. Peberdy, A. Rodger, J.O. Trent, P.J. Bates, Biophysical and biological properties of quadruplex oligodeoxyribonucleotides, Nucleic Acids Res. 31 (2003) 2097-2107.
[30] M. Scuotto, E. Rivieccio, A. Varone, D. Corda, M. Bucci, V. Vellecco, G. Cirino, A. Virgilio, V. Esposito, A. Galeone, N. Borbone, M. Varra, L. Mayol, Site specific replacements of a single loop nucleoside with a dibenzyl linker may switch the activity of TBA from anticoagulant to antiproliferative, Nucleic Acids Res. 43 (2015) 7702-7716.
[31] V. Esposito, A. Russo, T. Amato, M. Varra, V. Vellecco, M. Bucci, G. Russo, A. Virgilio, A. Galeone, Backbone modified TBA analogues endowed with antiproliferative activity, Biochim. Biophys. Acta, Gen. Subj. 1861 (2017) 1213-1221.
[32] L. Deng, Y. Du, J.-J. Xu, H.-Y. Chen, An off–on–off electrochemiluminescence approach for ultrasensitive detection of thrombin, Biosens. Bioelectron. 59 (2014) 58-63.
[33] S.Y. Tan, C. Acquah, A. Sidhu, C.M. Ongkudon, L. Yon, M.K. Danquah, SELEX modifications and bioanalytical techniques for aptamer–target binding characterization, Crit. Rev. Anal. Chem. 46 (2016) 521-537.
[34] M.Á. Corral-Rodríguez, P.E. Bock, E. Hernández-Carvajal, G.-G. R., P. Fuentes-Prior, Structural basis of thrombin-mediated factor V activation: the Glu666-Glu672 sequence is critical for processing at the heavy chain–B domain junction, Blood 117 (2011) 7164-7173.
[35] N. Venkatesan, B.H. Kim, Peptide conjugates of oligonucleotides: synthesis and applications, Chem. Rev. 106 (2006) 3712-3761.
[36] F.S. Hassane, A. Saleh, R. Abes, M. Gait, B. Lebleu, Cell penetrating peptides: overview and applications to the delivery of oligonucleotides, Cell. Mol. Life Sci. 67 (2010) 715-726.
[37] K. Ohtsuka, S. Sato, Y. Sato, K. Sota, S. Ohzawa, T. Matsuda, K. Takemoto, N. Takamune, B. Juskowiak, T. Nagai, Fluorescence imaging of potassium ions in living cells using a fluorescent probe based on a thrombin binding aptamer–peptide conjugate, Chem. Commun. 48 (2012) 4740-4742.
[38] S.K. Panigrahi, G.R. Desiraju, Strong and weak hydrogen bonds in the protein–ligand interface, Proteins 67 (2007) 128-141.
[39] M.D. Hanwell, D.E. Curtis, D.C. Lonie, T. Vandermeersch, E. Zurek, G.R. Hutchison, Avogadro: An advanced semantic chemical editor, visualization, and analysis platform, J. Cheminf. 4 (2012) 1-17.
[40] Avogadro: an open-source molecular builder and visualization tool. Version 1.XX. http://avogadro.cc/.
[41] A. Ellington, J.D. Pollard Jr, Synthesis and purification of oligonucleotides, Curr. Protoc. Mol. Biol. 42 (1998) 2-11.
[42] S.M. Ocampo, F. Albericio, I. Fernández, M. Vilaseca, R. Eritja, A straightforward synthesis of 5'-peptide oligonucleotide conjugates using N(alpha)-Fmoc-protected amino acids, Org. Lett. 7 (2005) 4349-4352.

[43] C.S. Huertas, A. Aviñó, C. Kurachi, A. Piqué, J. Sandoval, R. Eritja, M. Esteller, L.M. Lechuga, Label-free DNA-methylation detection by direct ds-DNA fragment screening using poly-purine hairpins, Biosens. Bioelectron. 120 (2018) 47-54.
[44] E. Vanquelef, S. Simon, G. Marquant, E. Garcia, G. Klimerak, J.C. Delepine, P. Cieplak, F.Y. Dupradeau, R.E.D. Server: a web service for deriving RESP and ESP charges and building force field libraries for new molecules and molecular fragments, Nucleic Acids Res. 39 (2011) W511-517.
[45] J.A. Maier, C. Martinez, K. Kasavajhala, L. Wickstrom, K.E. Hauser, C. Simmerling, ff14SB: improving the accuracy of protein side chain and backbone parameters from ff99SB., J. Chem. Theory Comput. 11 (2015) 3696-3713.
[46] N. Eswar, B. Webb, M.A. Marti-Renom, M.S. Madhusudhan, D. David Eramian, M. Shen, U. Pieper, A. Sali, Comparative protein structure modeling using Modeller, Curr. Protoc. Bioinformatics 15 (2006) 5-6.
[47] W.L. Jorgensen, J. Chandrasekhar, J.D. Madura, R.W. Impey, M.L. Klein, Comparison of simple potential functions for simulating liquid water, The J. Chem. Phys. 79 (1983) 926-935.
[48] J.P. Ryckaert, G. Ciccotti, H.J.C. Berendsen, Numerical integration of the cartesian equations of motion of a system with constraints: molecular dynamics of n-alkanes, J. Comput. Phys. 23 (1977) 327-341.
[49] U. Essmann, L. Perera, M.L. Berkowitz, T. Darden, L. H., L.G. Pedersen, A smooth particle mesh Ewald method, J. Chem. Phys. 103 (1995) 8577-8593.
[50] Laboratory for Advanced Computing, University of Coimbra, http://www.lca.uc.pt.
[51] D.A. Case, T.E. Cheatham, T. Darden, H. Gohlke, R. Luo, K.M. Merz, A. Onufriev, C. Simmerling, B. Wang, R.J. Woods, The Amber biomolecular simulation programs, J. Comput. Chem. 26 (2005) 1668-1688.
[52] J.-L. Mergny, L. Lacroix, Analysis of thermal melting curves, Oligonucleotides 13 (2003) 515-537.
[53] S. Burge, G.N. Parkinson, P. Hazel, A.K. Todd, S. Neidle, Quadruplex DNA: sequence, topology and structure, Nucleic Acids Res. 34 (2006) 5402-5415.
[54] K. Padmanabhan, A. Tulinsky, An ambiguous structure of a DNA 15-mer thrombin complex, Acta crystallogr. D Biol. Crystallogr. 52 (1996) 272-282.
[55] I. Gomez-Pinto, E. Vengut-Climent, R. Lucas, A. Aviñó, R. Eritja, C. González, J.C. Morales, Carbohydrate-DNA interactions at G-quadruplexes: folding and stability changes by attaching sugars at the 5'-end, Chem. Eur. J. 19 (2013) 1920-1927.
[56] A. Virgilio, L. Petraccone, V. Vellecco, M. Bucci, M. Varra, C. Irace, R. Santamaria, A. Pepe, L. Mayol, V. Esposito, A. Galeone, Site-specific replacement of the thymine methyl group by fluorine in thrombin binding aptamer significantly improves structural stability and anticoagulant activity, Nucleic Acids Res. 43 (2015) 10602-10611.
[57] N. Pozzi, L. Acquasaliente, R. Frasson, A. Cristiani, S. Moro, A. Banzato, V. Pengo, G.L. Scaglione, A. Arcovito, R. De Cristofaro, β2-G lycoprotein I binds to thrombin and selectively inhibits the enzyme procoagulant functions, J. Thromb. Haemost. 11 (2013) 1093-1102.
[58] P.-H. Lin, R.-H. Chen, C.-H. Lee, Y. Chang, C.-S. Chen, W.-Y. Chen, Studies of the binding mechanism between aptamers and thrombin by circular dichroism, surface plasmon resonance and isothermal titration calorimetry, Colloids and Surf. B: Biointerfaces 88 (2011) 552-558.

[59] L.G. Carrascosa, A. Calle, L.M. Lechuga, Label-free detection of DNA mutations by SPR: application to the early detection of inherited breast cancer, Analy. bioanal. Chem 393 (2009) 1173-1182.
[60] V. Viglasky, T. Hianik, Potential uses of G-quadruplex-forming aptamers, Gen. Physiol. Biophys. 32 (2013) 149-172.
[61] L. Coelho, J.M.M.M. de Almeida, J.L. Santos, P.A. da Silva Jorge, M.C.L. Martins, D. Viegas, R.B. Queirós, Aptamer-based fiber sensor for thrombin detection, J. Biomed. Opt. 21 (2016) 1-9.
[62] C. Jiang, T. Zhao, S. Li, N. Gao, Q.-H. Xu, Highly sensitive two-photon sensing of thrombin in serum using aptamers and silver nanoparticles, ACS Appl. Mater Interfaces 5 (2013) 10853-10857.
[63] S. Wan, B. Knapp, D.W. Wright, C.M. Deane, P.V. Coveney, Rapid, precise, and reproducible prediction of peptide-MHC binding affinities from molecular dynamics that correlate well with experiment, J. Chem. Theory Comput. 11 (2015) 3346-3356.
[64] F. Chen, H. Sun, J. Wang, F. Zhu, H. Liu, Z. Wang, T. Lei, T. Li, T. Hou, Assessing the performance of MM/PBSA and MM/GBSA methods. 8. Predicting binding free energies and poses of protein-RNA complexes, RNA (2018) 1183-1194.
[65] S. Genheden, U. Ulf Ryde, The MM/PBSA and MM/GBSA methods to estimate ligand-binding affinities, Expert Opin. Drug discovery 10 (2015) 449-461.
[66] M. Aldeghi, A. Heifetz, M.J. Bodkin, S. Knapp, P.C. Biggin, Predictions of ligand selectivity from absolute binding free energy calculations, J. Am. Chem. Soc. 139 (2017) 946-957.
[67] S. Nagatoishi, N. Isoro, K. Tsumoto, N. Sugimoto, "Loop residues of thrombin-binding DNA aptamer impact G-quadruplex stability and thrombin binding., Biochimie 93 (2011) 1231-1238.
[68] B. Cai, X. Yang, L. Sun, X. Fan, L. Li, H. Jin, Y. Wu, Z. Guan, L. Zhang, L. Zhang, Z. Yang, Stability and bioactivity of thrombin binding aptamers modified with D-/L-isothymidine in the loop regions, Org. Biomol. Chem. 12 (2014) 8866-8876.
[69] T.B. Jensen, J.R. Henriksen, B.E. Rasmussen, L.M. Rasmussen, T.L. Andresen, J. Wengel, A. Pasternak, Thermodynamic and biological evaluation of a thrombin binding aptamer modified with several unlocked nucleic acid (UNA) monomers and a 2 '-C-piperazino-UNA monomer., Bioorg. Med. Chem. 19 (2011) 4739-4745.
[70] S. Goji, J. Matsui, Direct detection of thrombin binding to 8-bromodeoxyguanosine-modified aptamer: effects of modification on affinity and kinetics, J. Nucleic Acids 2011 (2011) 1-5.
[71] I. Russo Krauss, A. Merlino, C. Giancola, A. Randazzo, L. Mazzarella, F. Sica, Thrombin-aptamer recognition: a revealed ambiguity, Nucleic Acids Res. 39 (2011) 7858-7867.
[72] I. Russo Krauss, A. Merlino, A. Randazzo, E. Novellino, L. Mazzarella, F. Sica, High-resolution structures of two complexes between thrombin and thrombin-binding aptamer shed light on the role of cations in the aptamer inhibitory activity, Nucleic Acids Res. 40 (2012) 8119-8128.
[73] C.Y. Koh, S. Kumar, M. Kazimirova, P.A. Nuttall, U.P. Radhakrishnan, S. Kim, P. Jagadeeswaran, T. Imamura, J. Mizuguchi, S. Iwanaga, Crystal structure of thrombin in complex with S-variegin: insights of a novel mechanism of inhibition and design of tunable thrombin inhibitors, PloS One 6 (2011) 1-16.

[74] A.C. Figueiredo, D. de Sanctis, R. Gutiérrez-Gallego, T.B. Cereija, S. Macedo-Ribeiro, P. Fuentes-Prior, P.J.B. Pereira, Unique thrombin inhibition mechanism by anophelin, an anticoagulant from the malaria vector, Proc. Natl. Acad. Sci.109 (2012) E3649-E3658.

Appendix A. Supplementary data

Aptamer-peptide conjugates as a new strategy to modulate human α-thrombin binding affinity

Anna Aviñó[a,d], *Andreia F. Jorge*[b], *César S. Huertas*[c1], *Tânia F. G. G. Cova*[b], *Alberto Pais*[b], *Laura M. Lechuga*[c,d], *Ramon Eritja*[a,d,*] *and Carme Fabrega*[a,d,*]

[a]Institute for Advanced Chemistry of Catalonia (IQAC-CSIC), Jordi Girona 18-26, E-08034 Barcelona, Spain.

[b]CQC, Department of Chemistry, University of Coimbra, Rua Larga, 3004-535 Coimbra, Portugal.

[c]Catalan Institute of Nanoscience and Nanotechnology (ICN2), CSIC, ICN2 Building, Campus UAB, Bellaterra, 08193 Barcelona, Spain.

[d]Networking Center on Bioengineering, Biomaterials and Nanomedicine (CIBER-BBN), Jordi Girona 18-26, E-08034 Barcelona, Spain.

Table of contents:

1. **Material and methods**

1.1. Reagents

The standard ancillary reagents and phosphoramidites used on the TBA synthesis were obtained from Applied Biosystems and Link Technologies Ltd. 5'-MMT-Amino-Modifier C6-CE-phosphoramidite and 3'-Thiol-Modifier C3 S-S CPG were obtained from Link Technologies. Matrix for MALDI-TOF experiments was composed by 2',4',6'-trihydroxyacetophenone monohydrate (THAP, Aldrich) and ammonium citrate dibasic (Fluka). Solvents for HPLC analysis and purification were prepared using acetonitrile (Merck) and triethylammonium acetate (TEAA) as mobile phase. The Fmoc-glutamic acid and the Fmoc-Gly_3 were purchased to Novabiochem and the rest of amino acids to Sigma. The rest of the chemicals are analytical reagent grade from commercial sources as specified. Solvents used for gold sensor chip cleaning were purchased from Panreac Applichem (Barcelona, Spain): Acetone 99.5% and Ethanol 99%. Main salts and chemical reagents for all the experiments, sensor cleaning, buffer preparation and biofunctionalization were acquired from Sigma-Aldrich (Germany): sodium dodecyl sulfate (SDS), hydrochloric acid (HCl), sodium hydroxide (NaOH), sodium chloride (NaCl) ≥99.5%, potassium chloride (KCl) and Magnesium chloride ($MgCl_2$).

1.2. Instrumentation

Modified TBA sequence was synthesized on an ABI 3400 DNA Synthesizer (Applied Biosystems). Semipreparative and analytical RP-HPLC was performed on a Waters chromatography system using Nucleosil 120 C18 (250x8mm) and XBridge OST C_{18} respectively. Mass spectra data were recorded on a MALDI Voyager DE RP time-of-flight (TOF) spectrometer (Applied Biosystems). Absorption spectra between 220 and 300 nm and the melting temperatures at 295 were recorded with a Jasco V650 spectrophotometer equipped with a Peltier temperature-controlling unit. The temperature was controlled with an 89090A Agilent Peltier device. Hellma quartz cuvettes were used. CD spectra were recorded on a JASCO spectropolarimeter J-810. Polyacrylamide gels were imaged with a Gene Genius Bioimaging system (Syngene). Model building was performed in Avogadro. The home made SPR [75] sensor platform is based on Kretschmann configuration, monitoring the binding interaction in real time. A polarized light of 670 nm from a laser source is divided in two identical beams

focused on the crystal-backside of the sensor chip (glass surface coated with 2 nm of chromium and 45 nm of gold, 10×10×0.3 mm from SSens, Enschede – The Netherlands). The flow system consists of two flow cells (300 nL each) for two simultaneous and independent analysis. Measurements were performed at a fixed angle of incidence and the variations of the refractive index (RI) were detected in a multielement photodiode. The device incorporates all optics, electronics and fluidics components necessary to operate autonomously. Sensograms reproduce the binding event by monitoring the increase (or decrease in case of unbinding events) of the intensity of the reflected light (ΔReflectivity (%), ΔR (%)) vs. time (seconds, s). This change of the intensity of the reflected light is directly related to changes in the RI of the dielectric medium caused by mass changes on the metallic surface. Origin 8.0 software (OriginLab, Northampton, MA) is used to collect the data.

2. MD simulations

2.1. MM-GBSA analyses

The end-state calculation Generalized Born and surface area continuum solvation (MM-GBSA) method [76] was used to obtain a detailed description of the α-thrombin/TBA interaction. Following this approach, the binding free energies were calculated according to:

$$\Delta G_{bind} = [G_{\alpha\text{-thrombin/15-TBA}}(X)] - [G_{\alpha\text{-thrombin}}(X)]\,[G_{15\text{-TBA}}(X)] \quad (1)$$

in which the parameters are estimated from frames, denoted as (x), taken from the replicate MD trajectories. For each frame, the free energy of a state is estimated by:

$$G(x) = H_{gas}(x) + H_{trans/rot}(x) + G_{solvation}(x) - TS(x) \quad (2)$$

Where H_{gas} (x) and $H_{trans/rot}$ (x) are calculated from internal (bond, angle, dihedrals), electrostatic and van der Waals energies. The $G_{solvation}$ (x) includes the input of polar and non-polar terms in which the polar contribution is typically obtained by using the generalized Born (GB) model whereas the non-polar tern is estimated from the solvent-accessible surface area (SASA) determined with the LCPO method. Finally, the last term, TS(x) corresponds to the

conformational entropy to the binding. MM-GBSA analyses were made with MMPBSA.py program in AMBER14 using the last 1000 frames from the equilibrated trajectory with a single trajectory approach. For MM-GBSA, a level-set-based dielectric model was used with an ionic strength equal 150 mM, and a solvent probe of 1.4 Å radii. The average values for binding energy are calculated from the 8 independent simulations. SEM values were calculated by the value of sample standard deviation divided by the square root of the total number of simulations.

2.2. Analysis and visualization of noncovalent interactions

The noncovalent interactions within α-thrombin/TBA complexes are evaluated resorting to the Independent Gradient Method (IGM)[3] and the IGMPlot software (version 1.0). These are specially useful for inspecting weak interactions in protein structures and related complexes [77-79]. IGM is ruled by the topological characteristics of the electronic charge density, ρ, of each system. In addition to $\boldsymbol{\rho}$, other relevant quantities related to the first and second derivatives of the density are considered. The IGM descriptor δg^{inter} is defined by the difference between the first derivatives of the charge densities for the total system and the fragments

$$\delta g^{\text{inter}} = |\nabla \boldsymbol{\rho}^{\mathbf{IGM,\ inter}}| - |\nabla \boldsymbol{\rho}| \qquad (1)$$

The presence of NCI is indicated by $\delta g^{\text{inter}}>0$ and the respective strength is reflected by the magnitude of the descriptor at a point in space. $\nabla^2 \boldsymbol{\rho}^{\mathbf{IGM,\ inter}}$ is calculated from sums over all the atomic densities in the different fragments denoted A and B in the x-direction,

$$\left(\frac{\delta \rho}{\delta x}\right)^{IGM,inter} = \left|\sum_{i=1}^{N_A} \frac{\delta \rho_i}{\delta x}\right| + \left|\sum_{i=1}^{N_B} \frac{\delta \rho_i}{\delta x}\right| \qquad (2)$$

IGMPlot uses the pre-computed atomic charge densities for constructing a promolecular density producing a minimal effect on the NCI, as in these extremely low-density regions a very little relaxation of the charge density occurs, following the formation of covalent bonds. Also, a discrimination between favorable and unfavorable NCI is dependent on the second derivative (Laplacian) of the density $\nabla^2 \boldsymbol{\rho}$, which can be decomposed into three eigenvalues of maximal variation, $\nabla^2 \boldsymbol{\rho} = \boldsymbol{\lambda_1} + \boldsymbol{\lambda_2} + \boldsymbol{\lambda_3}$ ($\boldsymbol{\lambda_1} \leq \boldsymbol{\lambda_2} \leq \boldsymbol{\lambda_3}$) providing information on the stabilizing ($\lambda_2< 0$) or destabilizing ($\lambda_2> 0$) interactions. Larger (negative) values of $\mathbf{sign}(\boldsymbol{\lambda_2})\boldsymbol{\rho}$ reflect stronger

interactions, such as hydrogen bonds, while **sign(λ_2)ρ** values close to zero are associated to weak NCI including van der Waals forces. Specifically, the coordinates of the each complex were extracted from last frame of the simulations that presents a free energy value closest to the free energy mean value. Solvent molecules were removed and the complexes were dissociated into the respective binding components (thrombin/TBA, thrombin/peptide, peptide/TBA). NCI are represented in space by isosurface volumes for the δg^{inter} colored according to the values of **sign(λ_2)ρ** at each point on the surface. This allows inferring on the (de)stabilizing nature and extent of the interactions. The preparation and representation of the systems and isosurface graphics were carried out using the Visual Molecular Dynamics software version 1.9.2. [80] A quantitative evaluation of the types and strengths of NCI within the complexes was assured by combining the isosurface representations and the values of the same two descriptors.

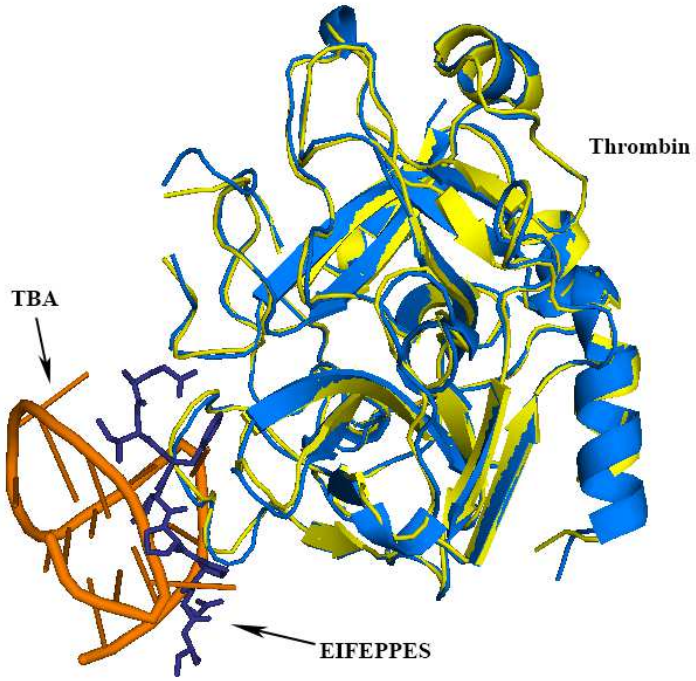

Supplementary Figure 1. Superposition of the two crystal structures of human α-thrombin bound to the TBA (PDB ID: 1HAO) and to the peptide (EIFEPPES) ((PDB ID: 3PZ6). α-thrombin are colored in yellow and blue, TBA in orange and the peptide sequence in dark blue. α-thrombin structures are represented by the secondary structure elements (new ribbons representation), the TBA is represented in cartoon and the peptide is represented in sticks.

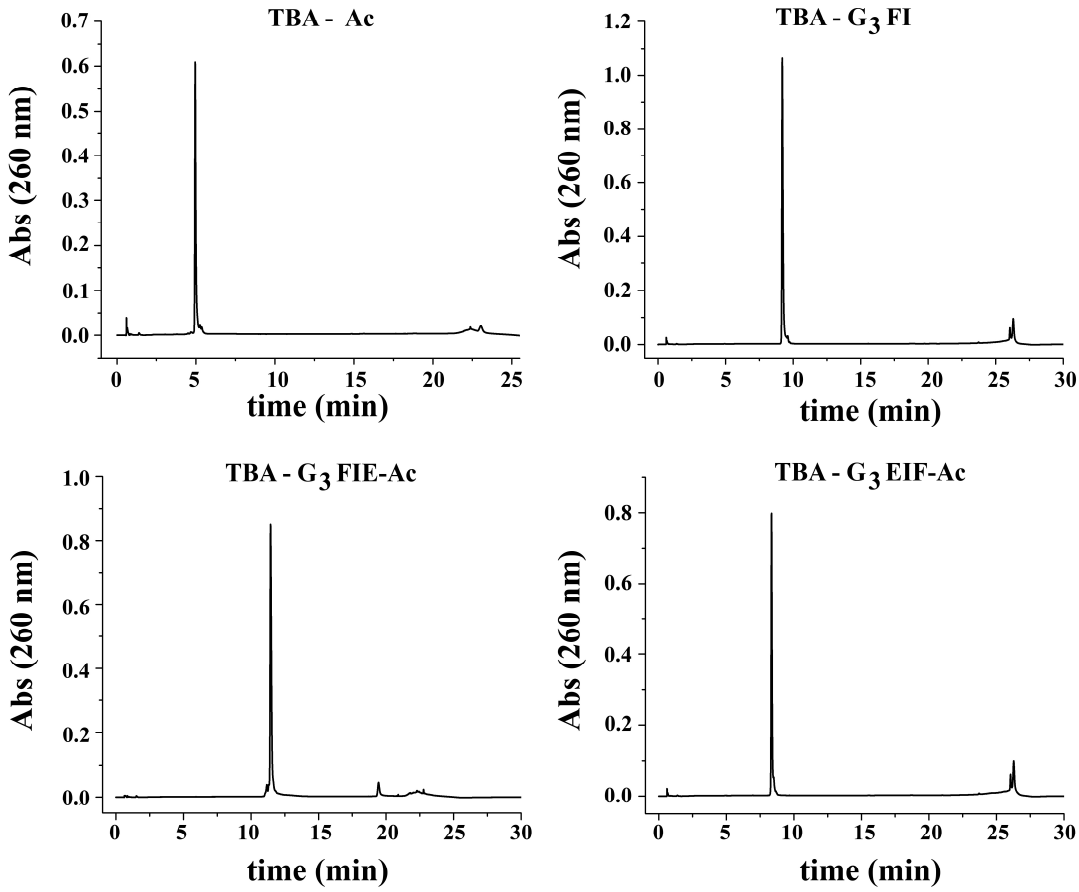

Supplementary Figure S2. HPLC analytical profiles of the different product obtained conjugate (XBridge OST C_{18} column).

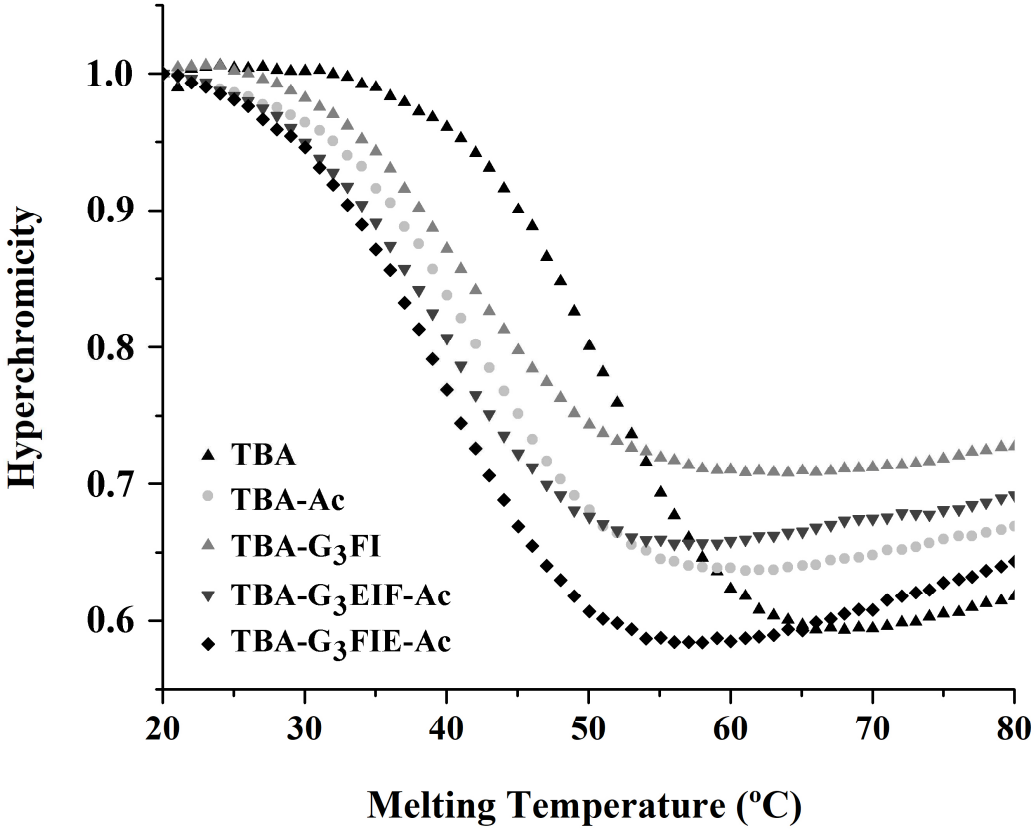

Supplementary Figure 3. Melting temperatures profile of the different oligonucleotide-peptide conjugates. The samples were in 10 mM sodium cacodylate pH 7.0 and 100 mM KCl and were heated over the range 20-80 °C.

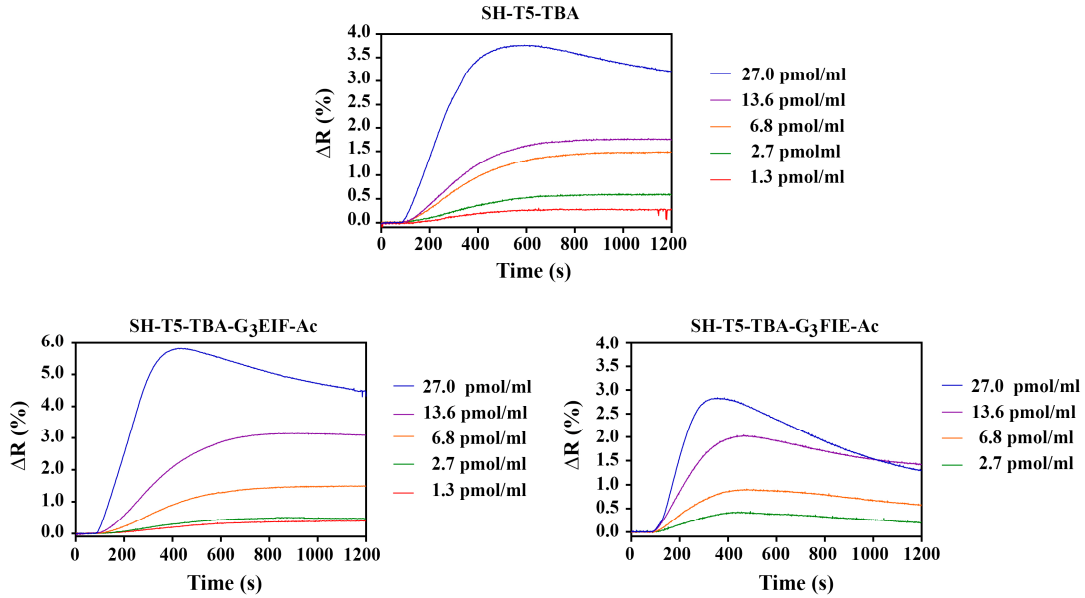

Supplementary Figure 4. SPR raw data of the experiments shows the interaction between α-thrombin and TBA-peptide conjugates variant. 1 μM TBA-peptide in the following solution (20 mM Tris pH 7.4, 140 mM NaCl, 5 mM KCl, 1 mM $MgCl_2$) was immobilized and different concentrations (from 0.01 to 1 μM) of α-thrombin were flowed in, using the same buffer at a 16 μL min^{-1} and at rt.

A α-thrombin/TBA

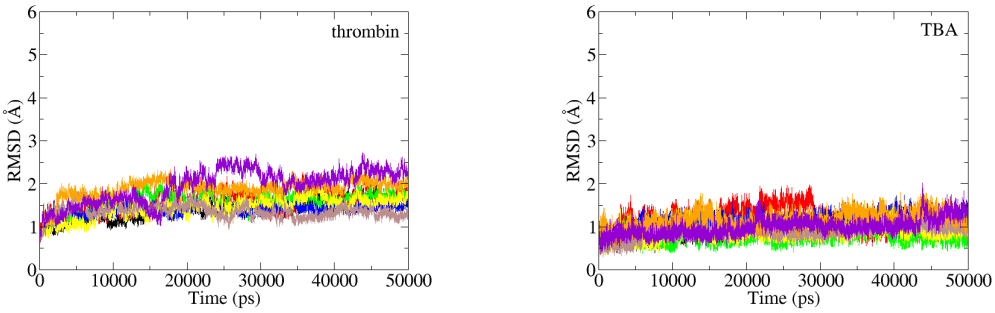

B α-thrombin/TBA-G_3FIE-Ac

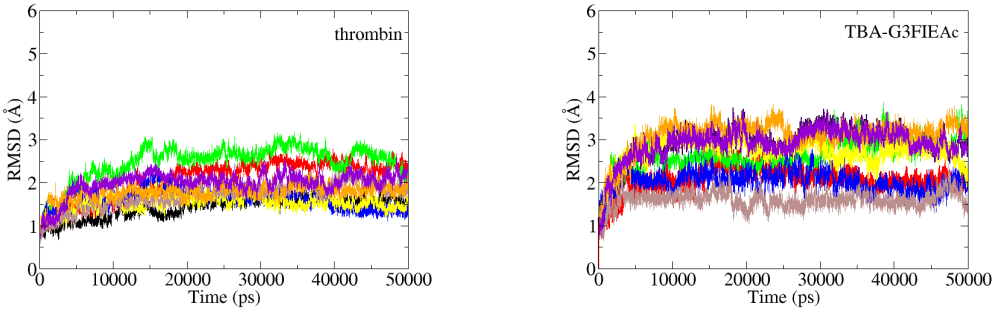

C α-thrombin/TBA-G_3EIF-Ac

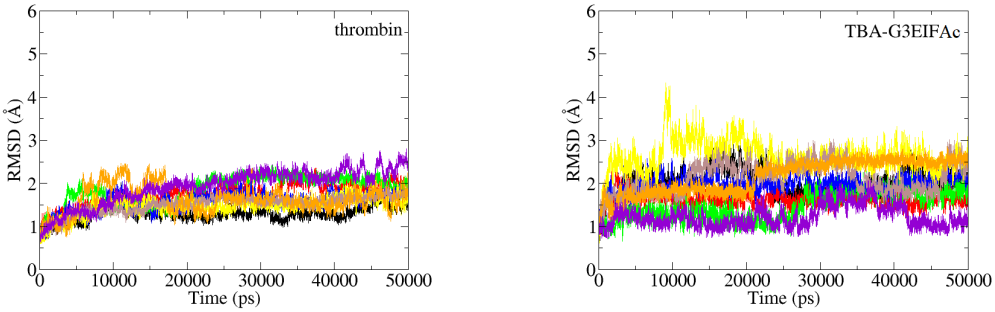

Supplementary 5. Structural variations for the (A) α-thrombin/TBA, (B) α-thrombin/TBA-G_3FIE-Ac and (C) α-thrombin/TBA-G_3EIF-Ac simulation systems obtained MD simulations. The structural behavior of α-thrombin and the three aptamers is shown separately. The heavy atoms belonging to thrombin backbone (Cα) and to TBA (P, O3', O5', C3', C4', C5') were

selected for carry out the root-mean-square-deviation (RMSD) analyses, taking the first frame of the production run as the RMSD reference. The RMSD values for the eight replicates are compiled in each graph.

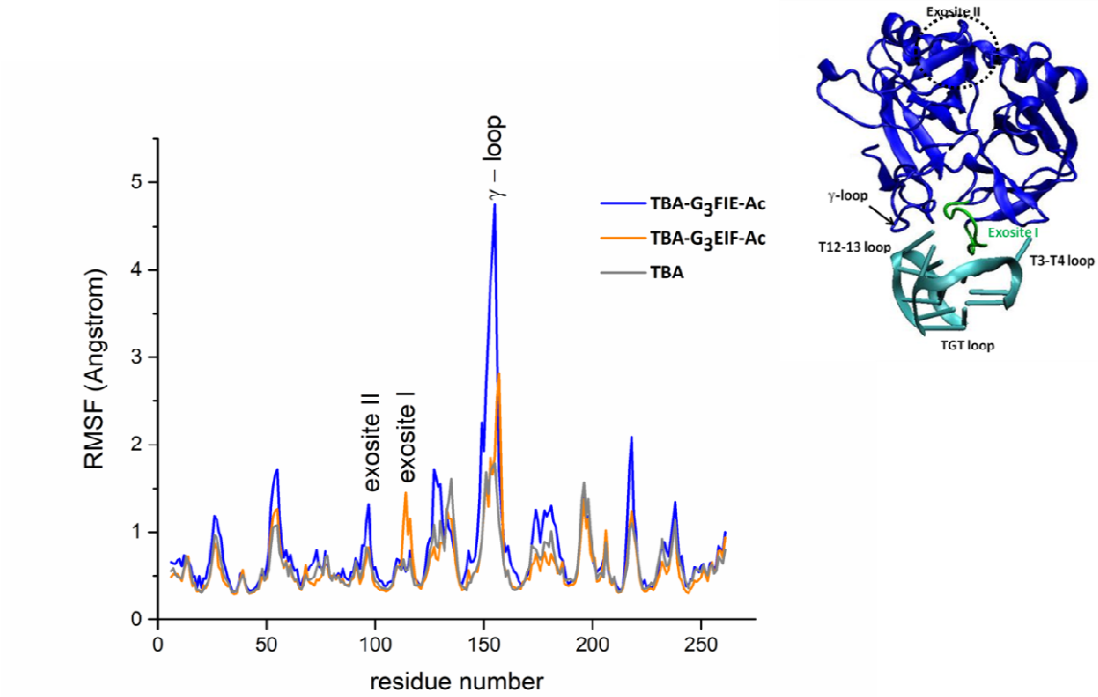

Supplementary Figure 6. Root-mean-square-fluctuation (RMSF) relative to the reference structure for the backbone atoms of human α-thrombin bound to natural TBA and the modified aptamers TBA-G_3EIF-Ac and TBA-G_3FIE-Ac. The curves represent the average value of RMSF obtained from 8 MD simulations, considering the last 10 ns of production run. The main secondary structures are depicted in correspondence to protein residue number.

Supplementary Table 1. Binding free energy calculated by MM-GBSA methodology and its components of α-thrombin/TBA, α-thrombin/TBA-G_3FIE-Ac and α-thrombin/TBA-G_3EIF-Ac complexes obtained in eight replicates. Data are provided in kcal mol^{-1}.

Systems	Replicates	ΔE_{vdw}	ΔE_{ELE}	ΔE_{GB}	ΔEsurf	ΔG_{pol} [b]	ΔG_{nonpol} [c]	ΔG_{bind} [d]	TΔS	ΔG(ΔΔG) [e]
TBA	rep1	-59.6	-1409.50	1414.8	-6.5	5.3	-66.1	-60.8	-40.3	-20.5
	rep2	-81.1	-1454.9	1475.4	-9.5	20.4	-90.6	-70.2	-40.03	-30.1
	rep3	-45.0	-1484.2	1483.5	-4.8	-0.7	-49.8	-50.5	-35.8	-14.7
	rep4	-60.8	-1363.9	1376.7	-6.6	12.8	-67.4	-54.5	-36.9	-17.6
	rep5	-59.9	-1437.9	1435.0	-6.1	-2.9	-66.0	-68.9	-27.9	-40.9
	rep6	-63.5	-1389.1	1394.2	-7.0	5.2	-70.5	-65.3	-38.7	-26.6
	rep7	-61.8	-1351.1	1351.8	-7.0	0.7	-68.8	-68.1	-36.6	-31.5
	rep8	-68.4	-1516.0	1518.4	-7.5	2.4	-75.9	-73.5	-46.6	-26.8
	Average ± SEM	**-62.5±4.1**	**-1425.8±23.7**	**1431.2±23.5**	**-6.9±0.5**	**5.4±3.2**	**-69.4±4.6**	**-64.0±3.3**	**-37.9±2.1**	**-26.1±3.9**
TBA-G_3FIE-Ac	rep1	-63.5	-1608.5	1608.8	-6.9	0.3	-70.4	-70.1	-42.4	-27.7
	rep2	-39.5	-1477.4	1483.3	-4.7	5.9	-44.3	-38.4	-31.3	-7.1
	rep3	-76.1	-1596.1	1615.9	-9.1	19.9	-85.3	-65.4	-36.7	-28.7
	rep4	-35.8	-1521.6	1519.6	-4.2	-2.0	-40.0	-42.0	-29.5	-12.5
	rep5	-68.5	-1500.1	1526.4	-8.4	26.3	-76.9	-51.0	-47.0	-3.6
	rep6	-58.9	-1518.8	1528.1	-7.9	9.3	-66.7	-57.5	-33.2	-24.3
	rep7	-64.1	-1709.5	1714.2	-8.0	4.8	-72.1	-67.3	-38.4	-28.9
	rep8	-69.0	-1742.6	1747.7	-8.8	5.1	-77.8	-72.7	-38.6	-34.1
	Average ± SEM	**-59.4±5.9**	**-1584.3±40.3**	**1593.0±39.5**	**-7.2±0.8**	**8.7±4.0**	**-66.7±6.6**	**-58.0±5.4**	**-37.1 ± 2.4**	**-20.8±5.9**
TBA-G_3EIF-Ac	rep1	-47.4	-1658.1	1649.3	-5.7	-8.8	-53.1	-61.8	-32.8	-29.0
	rep2	-92.2	-1712.3	1717.9	-11.3	5.6	-103.6	-97.9	-42.7	-55.3
	rep3	-85.3	-1649.1	1663.8	-10.5	14.7	-95.7	-81.0	-45.9	-35.1
	rep4	-81.0	-1625.4	1634.4	-9.7	9.1	-90.7	-81.6	-46.0	-35.6
	rep5	-73.3	-1829.3	1810.8	-9.7	-18.5	-83.1	-101.6	-42.8	-58.8
	rep6	-95.6	-1870.2	1867.9	-11.5	-2.4	-107.2	-109.5	-62.9	-46.6
	rep7	-102.3	-1726.8	1736.5	-11.9	9.7	-114.2	-104.5	-38.4	-66.1
	rep8	-69.31	-1778.94	1786.85	-7.60	7.91	-76.91	-68.99	-42.2	-26.8
	Average ± SEM	**-80.8±7.1**	**-1731.3±36.2**	**1733.4±34.1**	**-9.7±0.9**	**2.2±4.6**	**-90.5±8.0**	**-88.4±7.2**	**-44.2±3.5**	**-44.1±8.0**

The symbols depicted in the table columns corresponds to: ΔE_{VDW}, van der Waals energy; ΔE_{ELE}, electrostatic energy; ΔE_{GB}, electrostatic contribution to the solvation free energy calculated by GB; ΔG_{SA}, non-polar contribution to the solvation free energy calculated with LCPO method; [b] $\Delta G_{pol} = \Delta E_{ELE} + \Delta G_{GB}$; [c] $\Delta G_{nonpol} = \Delta E_{VDW} + \Delta G_{SA}$; [d] $\Delta G_{bind} = \Delta E_{ELE} + \Delta E_{GB} + \Delta E_{VDW} + \Delta G_{SA}$; TΔS, total entropy contribution; [e] $\Delta G(\Delta\Delta G) = \Delta G - T\Delta S$. ΔG(ΔΔG) is the total free energy.

3. References

[1] A. Aviñó, C.S. Huertas, L.M. Lechuga, R. Eritja, Sensitive and label-free detection of miRNA-145 by triplex formation, Analytical and bioanalytical chemistry, 408 (2016) 885-893.
[2] P.A. Kollman, I. Massova, C. Reyes, B. Kuhn, S. Huo, L. Chong, M. Lee, T. Lee, Y. Duan, W. Wang, Calculating structures and free energies of complex molecules: combining molecular mechanics and continuum models, Accounts of chemical research, 33 (2000) 889-897.
[3] C. Lefebvre, G. Rubez, H. Khartabil, J.-C. Boisson, J. Contreras-García, E. Hénon, Accurately extracting the signature of intermolecular interactions present in the NCI plot of the reduced density gradient versus electron density, Physical Chemistry Chemical Physics, 19 (2017) 17928-17936.
[4] T.F. Cova, B.F. Milne, A.A. Pais, Host flexibility and space filling in supramolecular complexation of cyclodextrins: A free-energy-oriented approach, Carbohydrate polymers, 205 (2019) 42-54.
[5] T.n.F. Cova, B.F. Milne, S.C. Nunes, A.A. Pais, Drastic Stabilization of Junction Nodes in Supramolecular Structures Based on Host–Guest Complexes, Macromolecules, 51 (2018) 2732-2741.
[6] W. Humphrey, A. Dalke, K. Schulten, VMD: visual molecular dynamics, Journal of molecular graphics, 14 (1996) 33-38.